

CHALMERS



Radar Target Altitude Measurement Evaluation of Different Optimization Algorithms

Master of Science Thesis

FABIAN LUNDBÄCK
VICTOR WAREBORN

Department of Signals and Systems
CHALMERS UNIVERSITY OF TECHNOLOGY
Gothenburg, Sweden, 2013
Report No. EX019/2013

REPORT NO. EX019/2013

Radar Target Altitude Measurement

Evaluation of Different Optimization Algorithms

FABIAN LUNBÄCK
VICTOR WAREBORN

Department of Signals and Systems
CHALMERS UNIVERSITY OF TECHNOLOGY
Göteborg, Sweden 2013

Radar Target Altitude Measurement
Evaluation of Different Optimization Algorithms
FABIAN LUNDBÄCK
VICTOR WAREBORN

©FABIAN LUNDBÄCK
VICTOR WAREBORN, 2013.

Department of Signals and Systems
Chalmers University of Technology
SE-412 96 Gothenburg
Sweden
Telephone +46(0)31-772 1000

Göteborg, Sweden 2013

Radar Target Altitude Measurement
Evaluation of Different Optimization Algorithms
FABIAN LUNDBÄCK
VICTOR WAREBORN
Department of Signals and Systems
Chalmers University of Technology

ABSTRACT

When a flying target is detected by airborne radar it is common that specular reflections occurs from smooth surfaces of the Earth, such as oceans and lakes. In the radar input signal, these reflective echoes are considered as pulses containing information about the detected targets altitude above the ground. In this project a curve fit to this input signal is applied, aligned with a Least-Squares Estimation, LSE. As a number of curve fits have been carried out, it is desired to find the minimum LSE-loss function value, i.e. the signal fit that gave the least-squares error. When this minimum is found, it is possible to determine the targets altitude. Because of a heavy computational burden some simplifications are made, meanwhile optimization methods, such as Gauss Newton with line search, GN, Steepest Descent with line search, SD, and Numerical Neighborhood search, NN, are applied to find local minima in a discrete search space composed by the LSE-loss function values. The results have shown that the method can fit curves for severe cases when pulses begin to interact, while a high noise level characterizes the input signal. With some simplifications and using a combination of GN and NN has resulted in a reduction of the computational time by 470,9 times, while 95,9% of the global minima in the LSE-loss functions discrete estimation space are found in a special case scenario.

Index Terms: *Curve/Data Fitting, Gauss Newton, Least-Squares Estimate, Non-Linear Optimization, Radar Altitude Measurement, Steepest Descent.*

SAMMANFATTNING

Då ett flygande mål upptäcks av en flygburen radar kan speglingsreflektioner från släta jordytor uppstå. I radarns insignal kan dessa reflekterande ekon betraktas som pulser som innehåller information om det upptäckta målets höjd över marken. I detta projekt har en kurvanpassning till denna insignal anpassats med en minsta kvadrat estimering, LSE. Då flertalet kurvanpassningar har gjorts vill man hitta det lägsta funktionsvärdet, det vill säga den signal som givit det minsta kvadrat-felet. När detta minimum hittas kan man bestämma målhöjden. På grund av tung beräkningskraft har vissa förenklingar gjorts samtidigt som optimeringsmetoder, så som Gauss Newton med linjesökning, GN, steepest descent med linjesökning, SD, och numerisk grannsökning, NN, använts för att hitta lokala minima i en diskret sökrymd uppbyggd av LSE's funktionsvärden. Resultatet har visat att man med LSE kan anpassa kurvor för svåra fall då pulserna börjar flyta ihop, samtidigt som signalen präglas av en hög brusnivå. Med hjälp av en kombination av GN och NN har även beräkningstiden kunnat reduceras 470,9 gånger samtidigt som 95,9 % av de lägsta funktionsvärdena har hittats i den diskreta sökrymden för ett speciellt test-scenario.

Index Termer: *Gauss Newton, Ickelinjär optimering, Kurvanpassning, Minsta kvadrat estimering, Radarhöjdmätning, Steepest descent.*

ACKNOWLEDGEMENT

This work has been carried out with support from Saab Electronic Defence System (EDS) and the academic support given by the Department of Signals and Systems at Chalmers University of Technology.

Saab and the business area EDS is one of the world's premier suppliers of solutions for surveillance, threat detection and location, platform and force protection, as well as avionics. Saab Electronic Defence Systems has the bulk of its business in Kallebäck, Gothenburg.

The authors would like to express gratitude to all the devoted engineers in the project team at Saab EDS, foremost the supervisors Anders Larsson and Björn Hallberg as well as the recruiter Tomas Berling. Sincere thanks also goes to the supervisor Professor Tomas McKelvey at the Department of Signals and Systems.

Fabian Lundbäck & Victor Wareborn
Göteborg, Sweden 2013

NOMENCLATURE

Superscripts

$\mathbf{A}(\theta)$	Transfer matrix with radar geometrical properties and pulse-shape
A_k	Antenna diagram, where $k \in \{Transmitted\ lobe, Received\ up - lobe, Received\ down - lobe\}$
$A_{j,T}$	Normalized antenna gain amplitude factor at transmission
$A_{j,R}$	Normalized antenna gain amplitude factor at receiving
D	Approximation of the divergence factor
$\mathbf{g}_j(n)$	Signal characteristic for the direct echo
$\mathbf{g}'_j(n)$	Signal characteristic for the first multipath echo
$\mathbf{g}''_j(n)$	Signal characteristic for the second multipath echo
G	Gradient of the LSE-loss function
G_d	Ground range
G_{di}	Divided ground range, where $i = \{1, 2\}$
G_j	Normalized antenna gain amplitude factor for the direct echo
G'_j	Normalized antenna gain amplitude factor for the first multipath echo
G''_j	Normalized antenna gain amplitude factor for the second multipath echo
H_R	Radar altitude
H_T	Target altitude
I_0	Modified Bessel function
\mathbf{J}	Jacobian of the non-linear least-square problem
$\tilde{\mathbf{J}}$	Complex valued Jacobian
$\mathbf{L}(\theta_i)$	Concentrated LSE-loss function
\mathbf{L}_{lim}	Limit of LSE-loss function for convergence criteria

\mathbf{P}^\perp	Orthogonal projection to the complement to A 's column space
R_T	Range between radar and target
R_1	Range from radar to reflection point
R_2	Range from reflection point to target
R_e	Effective Earth radius
T_s	Sampling time interval
a	Amplitude
c	Microwaves propagation speed (Speed of light)
$h_{pc}(r)$	Pulse shape
$j \in \{u, d\}$	Represent up- and down beam
m_{max}	Maximum iterations for the Gauss-Newton algorithm
\mathbf{n}	Gaussian colored noise
n_0	Number of range bins collected before detected bin
nr	Number of measurements
r_3	Pulses 3 dB bandwidth
r_s	Sampling range interval
r_f	Range between sampled and true amplitude
\mathbf{s}	Target amplitude
$\hat{\mathbf{s}}$	Estimate of target amplitude
ss	Sea state
\mathbf{x}	Input signal
α	Step size in the Gauss-Newton line search
α_1	Angle between radar and reflection point
α_2	Angle between reflection point and target
$\theta_{\mathbf{d}}$	Angle between target and radar
θ	Estimation parameter vector
θ_b	Elevation angle, where $b = \{r, d\}$
θ_{lim}	Limit of estimation parameter for convergence criteria

$\theta_{\mathbf{gmin}}$	Estimation parameter for the lowest found minimum
$\theta_{\mathbf{lmin}}$	Estimation parameter for the second lowest found minimum
$\theta_{\mathbf{opt}}$	Estimation parameter for a found local minimum
θ_r	Angle between radar and Earth
δ_R	Range between direct- and second multipath echo
$\delta\theta$	Gauss-Newton search direction
τ_s	Time between transmitting and receiving a pulse
σ_e	Conductivity
σ_h	Standard deviation of the amplitude distribution for sea waves
ρ	Reflection factor of sea surface
ε_r	Ordinary dielectric constant
λ_r	Radar wavelength
$\epsilon(\theta)$	Least-squares residual
ψ	Grazing angle
$\frac{\partial}{\partial\theta}$	Derivative with respect to the parameter, θ
$(\cdot)^H$	Hermitian transpose, i.e. transpose and complex conjugation
$(\cdot)^T$	Transpose
$\ \cdot\ $	Norm

Abbreviations

DB	Down Beam
GN	Gauss Newton with line search
LSE	Least-Squares Estimation
NN	Numerical Neighborhood search
PRF	Pulse repetition frequency
RCS	Radar Cross Section
SD	Steepest Descent with line search
SNR	Signal to Noise Ratio
STD	Standard Deviation

TGS-ns	Total Grid search without saved data
TGS-s	Total Grid search with saved data
UB	Up Beam
QI	Quality Index
mhos	Electrical conductance, 1 A/V

Contents

1	INTRODUCTION	1
1.1	Radar Background	1
1.2	Multipath Background	4
1.3	Background for Pre-Saved Data	5
1.4	Background for Search Methods on a Non-Linear Least-Squares Problem	6
1.5	Motivations and Objectives	7
1.6	Allocated Limits	8
1.6.1	Hardware Limits	8
1.6.2	Input Signal Limits	9
2	METHOD & THEORY	10
2.1	Model	10
2.1.1	Environmental Model	10
2.1.1.1	<i>Target Model</i>	10
2.1.1.2	<i>Geometrical Model</i>	13
2.1.1.3	<i>Doppler Model</i>	16
2.1.1.4	<i>Reflection Model</i>	16
2.1.1.5	<i>Radar Model</i>	18
2.1.2	Model on Matrix Form	19
2.1.3	Model Simplifications	22
2.2	Least-Squares Estimate (LSE)	23
2.3	Numerical Search Methods	25
2.3.1	Total Grid Search (TGS)	26
2.3.2	Numerical Neighborhood Search (NN)	26
2.3.3	Gauss Newton with Line Search (GN)	27
2.3.4	Steepest Descent with Line Search (SD)	29
2.3.5	GN with NN	30
2.3.6	Number of Starting Points	30
2.4	General Extensions	31
2.4.1	Median of Several Estimations	31
2.4.2	Quality Index	31
2.4.3	Performance of Pulse Separation and Signal to Noise Ratio	32
2.4.4	Computational Burden	33
3	RESULTS	34
3.1	Creation of Input Signal	34
3.2	Calculation of Target Altitude from $\delta_{\mathbf{R}}$	35
3.3	Number of Starting Points Analysis	36
3.4	Numerical Search Methods	38
3.4.1	Total Grid Search (TGS)	38
3.4.1.1	<i>Comparison of Simplified- and Non-Simplified TGS with True Recorded Radar Signals</i>	38
3.4.1.2	<i>Interaction Between SNR and $\delta_{\mathbf{R}}$</i>	39

3.4.1.3	<i>Performance with Different SNR</i>	40
3.4.1.4	<i>Performance with 32 Median Measurements</i>	42
3.4.1.5	<i>Overview of Results for TGS-s</i>	43
3.4.2	Comparison of Different Search Methods	43
3.4.2.1	<i>Estimated δ_R Compared with True δ_R</i>	44
3.4.2.2	<i>Estimated H_T Compared with True H_T</i>	45
3.4.2.3	<i>Estimated H_T Compared with True H_T using Median of 32 Measurements</i>	46
3.4.2.4	<i>Difference Between TGS-s and the Optimization Search Methods</i>	47
3.4.2.5	<i>Summary of Results</i>	48
3.5	Quality Index (QI)	50
4	DISCUSSION	51
5	CONCLUSION	53
5.1	Results from Present Work	53
5.2	Future Work	53

1 INTRODUCTION

When using airborne radar to detect air targets over sea, a common problem that appears is that the transmitted pulses contribute to multipath received signals. Due to this radar effect of reflections over sea, or other smooth surfaces of the Earth, problems to identify targets have been a common phenomena that can occur. But if the multipath signals are known and emphasized instead of suppressed, it is possible to give a more accurate altitude measurement for the target, which is the focus of this project. After the received signal for the radar has been processed it may be considered as a pulse train with information of the multipath characteristic. When a signal is transmitted, this is done with different beam angles and a received beam is regarded as a pair of one up- and one down beam. This means that the input signal consist of two pulse trains, and with knowledge about the pulses mutual positions, a target altitude can be estimated.

This master thesis work will focus on the question if there is an algorithm that is fast enough and still give a good estimation of a targets altitude with respect to the multipath propagation. Previously the Least-Squares estimate (LSE) have been tested as a curve fitting method, and in this project the method will be evaluated and extended with the search methods Total Grid Search (TGS), Gauss Newton with line search (GN), Steepest Descent with line search (SD) and Numerical Neighborhood search (NN). The LSE-loss function is derived several times with different characteristic, where each value contributes to a curve fit error to the input signal. If these values are calculated over a total specified estimation space, a TGS is performed. The other search methods are then applied so that each value in the estimation space not needs to be derived. Important to notice is that the optimization problem is not continuous, but discrete.

1.1 Radar Background

A radar uses a sensor that transmits and receives electromagnetic energy in the form of microwaves. The pulses are transmitted by a powerful directional antenna. Between the pulses the antenna receives the reflected energy. By concentrating the radiated energy into a narrow beam and sweep through the expected region, it is possible to detect targets. The reflected energy can be from either targets, sea or land. The range to target can be calculated by the time it takes for the microwaves to travel from the radar to target and back again, and is derived by

$$R_T = \frac{c}{2\tau_s}, \quad (1)$$

where c is the microwaves propagation speed, i.e. speed of light, and τ the time

between the transmitted and received pulse [11].

Targets may be of different kinds but will hereafter be regarded as air targets.

Ideally when detecting targets the pulses should be as short as possible and at the same time send out as much energy as possible. This will give the highest probability to detect targets. Due to practical limitations of the peak power that the transmitting unit can deliver those requirements are contradictory. A solution to this dilemma is pulse compression. This is done by transmitting internally modulated pulses with a wider bandwidth to provide the necessary average power at a reasonable level of peak power. Then the received echo is compressed by decoding their modulation by a filter that fits the transmitted signal [11].

Transmitting and receiving is done coherently. These phase-coherence is of particular importance when movable targets should be determined near strong ground reflections and is of crucial importance to separate the received signal into two signals. One that occurs in phase with the transmitted signal and one 90 degrees phase-shifted. The separation is common called I/Q demodulation. When a pulse wave is reflected by a moving target the received pulse will contribute to a change in phase velocity, a so called doppler shift in frequency. By sensing the doppler frequencies the radar can separate target echoes from clutter and land, where objects with high radial velocity can be suppressed [11].

The number of pulses transmitted per second is called the pulse repetition frequency, PRF. The PRFs of airborne radars range is anywhere from a few hundred hertz to several kilohertz. The choice of PRF is crucial because it determines whether, and to what extent, the ranges and doppler frequencies observed by the radar will be ambiguous. Range ambiguities occur due to that the radar has no direct way of telling to which pulse a particular echo belongs. When PRF is low enough for all echoes from one pulse to be received before next pulse is transmitted, echoes will belong to the pulse that immediately precedes them. But if the PRF is high enough this wont be the case. Doppler ambiguities arises because of the discontinues nature of a pulsed signal. When a target is moving towards or away from the radar carrier a shift in I- and Q-channel will occur [11].

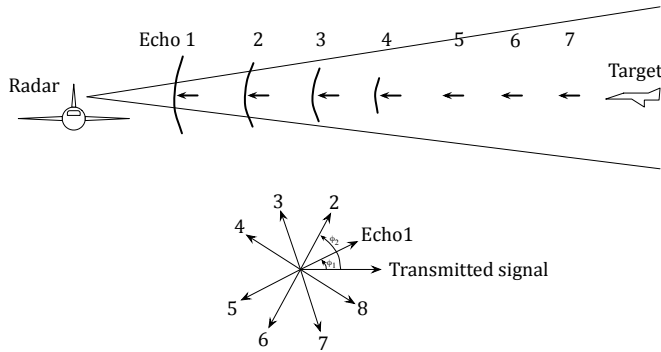


Figure 1: Target doppler frequency shows up as a pulse-to-pulse shift in phase.

A targets doppler frequency shows up as a progressive shift in the frequency phase, ϕ , of the received echoes from the target relative the transmitted pulses from the radar. This echo-to-echo phase shift is illustrated by a phase diagram in Fig. 1. By sensing the phase shift progressively it is possible to produce a signal whose amplitude fluctuates at the targets doppler frequency. Depending if the doppler frequency shift is positive or negative, Q will either lag or lead I by 90° respectively.

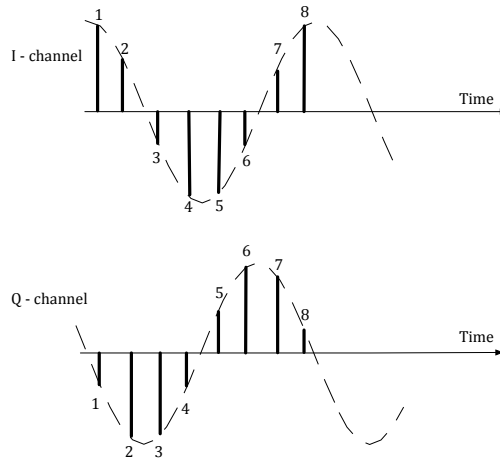


Figure 2: Doppler frequency with positive shift where both I and Q signal is provided. Notice that this is just an illustration.

One way of representing the received signal is by a range doppler matrix where the signal is mapped into two dimensions. In range dimension the matrix is separated in range bins where the range between the bins is equal to the sampling

range according to

$$r_s = \frac{c}{2T_s} \quad (2)$$

where T_s is the time between two samples. In doppler dimension the signal is separated into as many doppler channels as the doppler filter-bank allows [4].

From the received signal the following target properties can be extracted

- Range
- Radial velocity
- Elevation- and azimuth-direction
- Size

The radar will give exceptionally good values of range and velocity. The measurement for the direction to the target gives acceptable values, but it is difficult to obtain accurate values of the targets size [4].

1.2 Multipath Background

The multipath phenomena that occurs due to the multipath effect that arises when the Earth surface is smooth, especially when using airborne radar over oceans and lakes. This effect is normally seen as a problem when targets are detected, but if the multipath signals are known and emphasized instead of suppressed, it is possible to use this for target altitude measurements.

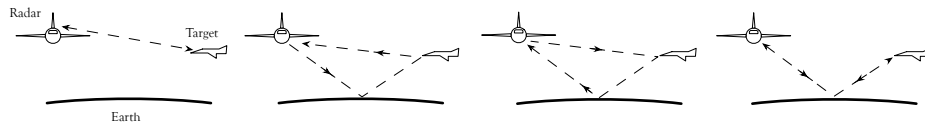


Figure 3: The four different cases of propagation for the radar signal during multipath effects.

The multipath signals can propagate in four different ways. This is illustrated in Fig. 3 where the first case is called the direct echo. Case 2 and 3 occurs at the same time, due to the same range for the radar pulses propagation, and can be seen as one case. This is called the first multipath echo. Case 4 is called the second multipath echo and contributes to the longest path.

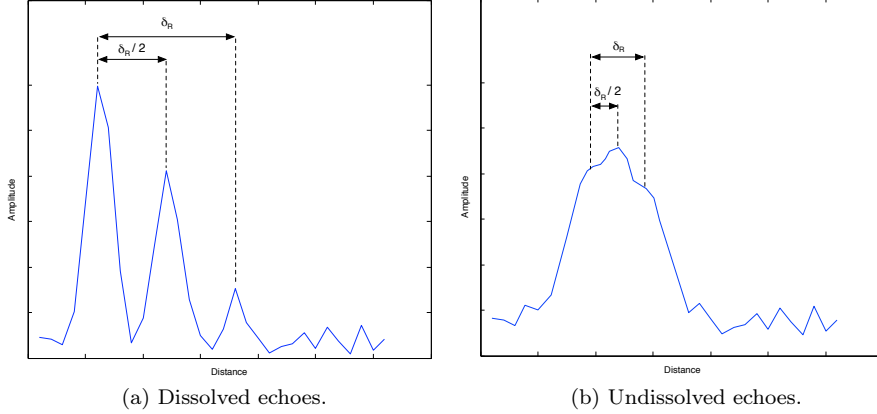


Figure 4: Two different beam signals received with multipath effect. Pulse 1,2 and 3 are the direct, first multipath and second multipath echo, respectively. δ_R can be seen as the range between the first- and third pulse for each beam.

Depending on how far away and at what altitude the target is positioned, different separations of the pulses in the input signal is obtained. Two possible characteristics from the radar when the multipath effect occurs is illustrated in Fig. 4. The first multipath echo is always located in between the direct echo and the second multipath echo. In the left graph (a) in Fig. 4, a signal where the echoes are completely resolved is illustrated and this can be seen as a simple case. When the target is far away and close to the Earth, the signal becomes less resolved and can be seen as a more difficult case. This is illustrated in the right graph (b) in Fig. 4.

When detecting the location of the pulses it is possible to determine the altitude. The estimated range between peak of direct echo and second multipath echo for a flat Earth model is approximately given by

$$\delta_R \approx \frac{2H_R H_T}{R_T} \quad (3)$$

where R_T is the range to the target, H_R the radar carrier altitude and H_T the target altitude. Depending on the positions of the target and the airborne radar, δ_R get its characteristic. If R_T becomes longer then the width of the received signal from the different echoes, or too small so the pulses overlaps, it can be impossible to determine it. Relationships for a spherical Earth is more complicated and explained in subsection 2.1.1.2 Geometrical Model.

1.3 Background for Pre-Saved Data

Because of the high computational burden for a TGS, simplifications and optimization methods are applied. Since the problem is not continuous but discrete

it is possible to predefine matrices used to derive the LSE-loss function values. Because of the discrete problem one can reduce the computational burden by mainly saving as much data as possible before each calculation. This means it is possible to extract matrices instead of derive complex equations. More about how this is used and how it effects the outcome is explained in subsection 2.1.3 and section 3.4, respectively.

1.4 Background for Search Methods on a Non-Linear Least-Squares Problem

One of the most common uses for the method of Least-Squares problems is in data fitting, or curve fitting. By finding a customized curve which matches the input data vector as well as possible one is able to find the input pulses mutual positions. More specifically, it is desired to find a vector of parameters that gives the “best fit” to the data by a model function [5]. The LSE-loss function is derived several times with different characteristic, where each value contributes to a curve fit error to the input signal. If these values are calculated over a total specified gridded estimation space, a TGS is performed. If all those values are assigned to a matrix, this can be seen as an estimation grid with two specified unknown parameters that should be estimated. The lowest value of the loss function over the discretized parameter space, the grid, will be the global optimum on the grid. The global optimum on the continuous parameter space will hence be located somewhere between the gridpoints. The difference in the parameter values between the global optimum and the grid optimum is thus upper bounded by the length between the gridpoints.

The next problem faced is to find the lowest grid value, i.e. the global grid minimum, without deriving each LSE-loss function values. The TGS will contribute to a high computational burden and instead a faster optimization algorithm needs to be implemented. An optimization problem can be expressed mathematically as the problem of determining an argument for which a given function has an extreme value, minimum or maximum, on a given domain. If not a TGS is used, finding a global minimum is difficult unless the problem has special properties. In most search methods local information, such as derivatives, are used and consequently are designated to find only a local minimum [5]. The concepts with global and local minimum for a one-dimensional problem are illustrated in Fig. 5.

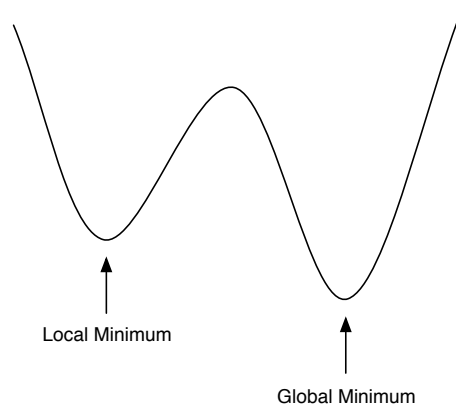


Figure 5: Local and Global minima.

When only local information is used there is usually no way to guarantee that a global minimum will be found using conventional numerical methods. Often the best is to start with an initial guess that is as close to the global minimum as possible and hope that the iterative solution process will converge to it. To increase the chance that a global minimum is found one might also try several different starting points, widely scattered throughout the feasible set. If they all produce the same result, then there is a good chance that a global minimum is found, and otherwise the best one can do is to take the lowest of the local minima found [5].

An important part that needs to be regarded is how the magnitude of the step should be defined for the optimized search methods. One alternative is to use a fixed step length and another approach is to alter the magnitude of the step using a line-search. Furthermore, it is reasonable to choose the step length such that the minimization function is approximately minimized. Most modern line-search implementations begin with a full Newton step, i.e. the step length gain is chosen to 1. Then estimates are computed until a step length is found that satisfies a sufficient decrease on the criterion function [1]. After each step, it is then inspected if any type of convergence criterion has been met, and if so, a local minimum seems to have been found.

1.5 Motivations and Objectives

The objective in this project is to evaluate and test different methods, approaches and algorithms that finds the altitude of a detected target. This is accomplished with help of the multipath effects that appears from the surface of the Earth. Since it is a complex problem the computational burden can be high, and a fast algorithm is needed. Therefore it is not only required to find a working algorithm, but also a fast one. The altitude measurement is assumed

to have succeeded when the pulses individual position, δ_R , in Fig. 4 is found. With this information it is possible to derive the estimated altitude. The pulses positions are found by using LSE as a curve fitting method which is evaluated using a TGS for the following matters:

- The ability to separate the pulses depending of how much they interact
- The ability to separate the pulses depending of how much noise the input data contains
- How much computational power that is required

In addition to that the LSE performance is evaluated, various methods are used to reduce the computational burden. The algorithm must be fast so it can be implemented in a real radar system. To decrease the computational burden simplifications and predefinitions can be made. Subsequently, it is investigated if the number of LSE-loss functions derived can further be reduced with other search methods

- GN
- SD
- NN

The result for the optimization search methods can then be compared to the TGS with respect to computational burden and performance.

If the target is close to the radar this will contribute to that the pulses are more separated. The focus in this project is especially to find a method that can detect the pulses when they are closely spaced. If the algorithm should handle well separated pulses this would require a greater search space, and therefore mainly targets at long ranges are analysed.

1.6 Allocated Limits

The allocated limits are separated in two areas; Hardware- and Input Signal Limits.

1.6.1 Hardware Limits

Because of high computational burden, consideration needs to be taken for the radars hardware limits, in terms of computation power and storage space. How effective the algorithm needs to be depends mostly of the Pulse Ratio Frequency, PRF. The altitude measurement needs to be finished at the same rate as the PRF. Notice that this is not entirely true when the frequency for each altitude measurement is reduced compared to the PRF.

1.6.2 Input Signal Limits

When the direct echo and multipath echoes are too close to each other there is a limit of how much they can interact before it is impossible to separate them. It is also impossible to separate the pulses from the echoes if the input signal contains too much noise.

Depending on how the search space is defined this limits how close and at what altitude the target can be. If the target is too close and too high, the pulse separation will exceed the input signal's vector dimensions.

When an altitude measurement is performed it is assumed that the range to the target is known, i.e. the position of the first pulse is assumed to be known.

2 METHOD & THEORY

This chapter describes all the background methods and theories for four different areas; Model, LSE, Search Methods and General Extensions.

2.1 Model

The model is divided into three main areas; Environmental, Matrix definitions and Simplifications.

2.1.1 Environmental Model

When the altitude should be estimated, it is important to develop a model that matches the true environmental impact, such as the radars soft- and hardware, geographic conditions and reflection properties. How this is defined are disclosed in the following subsection.

2.1.1.1 *Target Model*

The target can be modeled as a quantity of scatters over the extent of the targets geometrics. Each of these reflectors will contribute to incoming waves and consist of a large amount of signals. The sum of waves will of course occur with respect to relative phase. The reflectors will then interfere both constructively and destructively. If the surface of the target has a complicated geometrical shape, the target's scattering properties can not be described as deterministic.

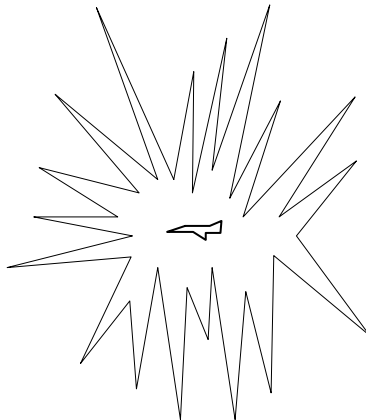


Figure 6: Target reflectors must be expressed in the model in terms of probabilities.

In the case when the target consist of a quantity of random scattered reflectors, illustrated in Fig. 6, the distribution function for the complex target amplitude is normal $N(0, \sigma_s)$ in real- and imaginary part. This gives that the Radar Cross Section ,RCS, is the square of target amplitudes and becomes exponential distributed. It also follows that the target amplitude with different radar wavelength is independent [4].

Angle Correlation

Due to that the total RCS is dependent on the individual reflectors relative position, the target area will fluctuate sharply with the angle to target with respect to the radar carrier.

When the multipath effect appears the radar will see the target from different incoming- and outgoing angles. This is illustrated in Fig. 7.

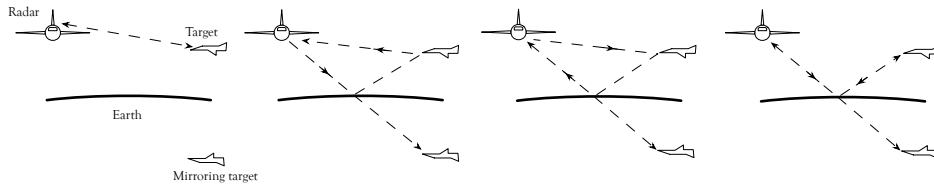


Figure 7: Four different possibilities for the radar wave path. The RCS in case 2 and 3 is considered to be identical while the target amplitudes for the other cases must not necessary be correlated.

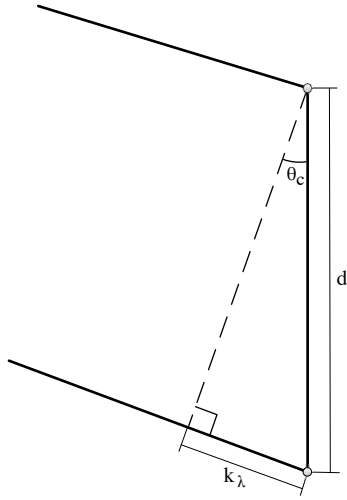


Figure 8: Targets main reflectors separated in altitude with range d .

The angle correlation can roughly be estimated from the model illustrated in Fig. 8. As described earlier the model will give a RCS pattern as in Fig. 6. When the target has two main reflection points separated in altitude with range d , difference in length is k_λ and the angle between the points is θ_c , as shown in Fig. 8. If the angle difference between the incoming waves from the two different reflection points is large, the correlation for the target area is considered to be zero. Since the target is big compared to the wavelength, the points are always considered as un-correlated. This means that every new pulse echo gets a new random value.

2.1.1.2 Geometrical Model

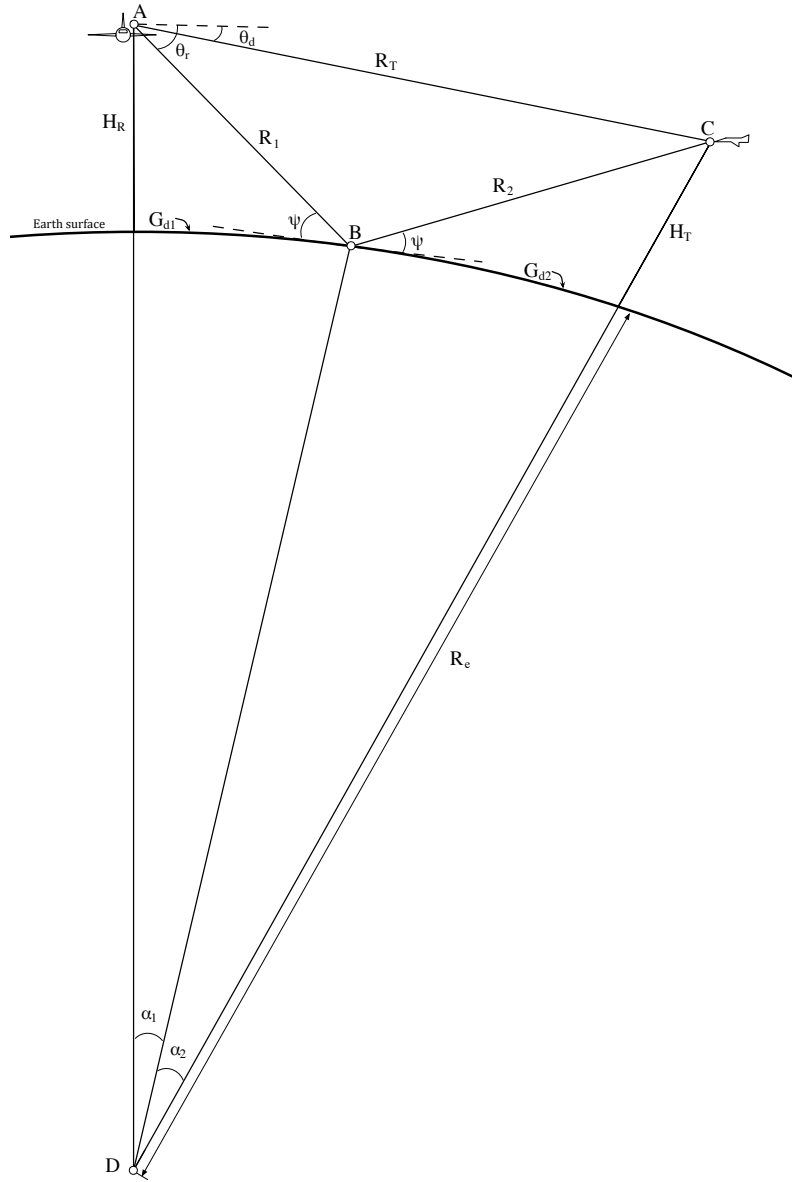


Figure 9: Geometry of spherical Earth reflection without restriction on altitude and range of target relative the radar.

The geometry model follows the one described in [2] and is used to derive the estimated altitude. To do this a model with spherical Earth is used, instead of the simplified with flat Earth explained in (3). How the model is defined is illustrated in Fig. 9. The basic problem is to define the correct reflection point given the ground range G_d , and this requires knowledge about how G_{d1} and G_{d2} are partitioned [2]. Assuming that target and radar altitude is much smaller than the effective Earth radius, R_e , the equation that must be solved is

$$2G_{d1}^3 - 3G_d G_{d1}^2 + [G_d^2 - 2R_e(H_R + H_T)] G_{d1} + 2R_e H_T G_d = 0 \quad (4)$$

where $R_e = \frac{4}{3} \cdot 6370$ km. The constant $\frac{4}{3}$ is used as a correction for the atmospheric refraction¹ [10].

When the range R_T is known instead of ground range G_d the following approximated equation needs to be solved

$$G_d \cong \sqrt{\frac{R_T^2 - (H_T - H_R)^2}{1 + \frac{(H_R + H_T)}{R_e}}}. \quad (5)$$

The range G_{d1} in (4) is given by

$$G_{d1} = \frac{G_d}{2} - p \sin\left(\frac{\xi}{3}\right) \quad (6)$$

where

$$p = \frac{2}{\sqrt{3}} \sqrt{R_e(H_R + H_T) + \left(\frac{G_d}{2}\right)^2} \quad (7)$$

and

$$\xi = \sin^{-1}\left(\frac{2R_e G_d (H_T - H_R)}{p^3}\right). \quad (8)$$

With G_{d1} given and if $G_{d2} = G_d - G_{d1}$, the angles α_1 and α_2 in Fig. 9 can be derived as

$$\alpha_1 = \frac{G_{d1}}{R_e}, \quad (9)$$

¹To further improve the accuracy of altitude computation refraction of the radar beam along the ray path to the target must be taken into account. Compared to free space where radar waves travels in straight lines, radar waves in the Earth's atmosphere generally are bent downward. The classical approach for atmospheric refraction in radar altitude computation applications is to replace the actual Earth radius by an effective Earth radius R_e . The use of the value $\frac{4}{3}$ has been widely adopted within the radar field [10].

$$\alpha_2 = \frac{G_{d2}}{R_e} \quad (10)$$

and

$$R_1 = \sqrt{H_R^2 + 4 R_e (R_e + H_R) \sin^2 \left(\frac{\alpha_1}{2} \right)}, \quad (11)$$

$$R_2 = \sqrt{H_T^2 + 4 R_e (R_e + H_T) \sin^2 \left(\frac{\alpha_2}{2} \right)}. \quad (12)$$

The elevation angle, θ_d , from the direct ray is exact calculated by applying the law of cosine to the triangle \overline{ABC} [2]

$$\theta_d = \sin^{-1} \left(\frac{2R_e(H_T - H_R) + H_T^2 - H_R^2 - R_T}{2(R_e + H_R)R_T} \right). \quad (13)$$

An approximation of θ_d can be used if, $H_T \ll R_e$ and $H_R \ll R_e$ as

$$\theta_d \cong \sin^{-1} \left(\frac{H_T - H_R}{R_T} - \frac{R_T}{2R_e} \right). \quad (14)$$

The depression angle of the reflected ray, θ_r , is found by similar analysis of triangle \overline{ABD} and can be approximated to

$$\theta_r \cong \sin^{-1} \left(\frac{H_R}{R_1} - \frac{R_1}{2R_e} \right). \quad (15)$$

θ_r is given by the angle with correct sign according to the geometrical model shown in Fig. 9, but must be negated to be used in the calculation of the antenna diagram.

δ_R can then be derived by [2]

$$\delta_R = R_1 + R_2 - R_T \quad (16)$$

but to avoid numerical calculation problems that may occur when large numbers are subtracted, the law of cosine is used and the final form of δ_R is

$$\delta_R = \frac{4 \left(H_R + \frac{H_R^2 - R_1^2}{2R_e} \right) \left(H_T + \frac{H_T^2 - R_2^2}{2R_e} \right)}{R_1 + R_2 + R_T}. \quad (17)$$

At a first sight it looks like a simple problem to derive H_T from (17), but note that both R_1 and R_2 contains highly nested expressions of H_T . How the final target altitude can be derived from δ_R , is described in section 3.2 Calculation of Target Altitude from δ_R .

2.1.1.3 *Doppler Model*

The doppler effect occurs due to that booth the target and radar is moving and the radio waves may be compressed or stretched in different ways. If the radar is closing on a target the wavelength is compressed and stretched if vice versa [11]. Because of the differences in elevation angle between the target and multipath targets, the radial velocity will not be consistent. For sufficiently large differences the target and the multipath targets will be separated into different doppler channels. If the angle θ_r in Fig. 9 is large, this will sometimes result in that the multipath target will be placed in another doppler channel than the direct target. In the model it is thus assumed that locations of the target occurs so that no separation is needed in the doppler dimension [4]. Since this project focus on targets far away, which contributes to a small θ_r , the problem rarely occurs, but it can still be regarded as a simplification.

2.1.1.4 *Reflection Model*

In the model it is assumed that the reflection arises from sea surfaces and is purely specular. The actual reflection-coefficients magnitude ρ , is regarded as the product of the three separate factors designated ρ_0 , ρ_s and D . Their total contribution is a number in the range from 0 to 1. This implies that the total specular reflection coefficient has a magnitude

$$\rho = \rho_0 \rho_s D \tag{18}$$

where

$$0 \leq \rho \leq 1. \tag{19}$$

ρ_0 is defined as the electromagnetic reflection coefficient of the material content that appears at the reflected surface. ρ_s is a spreading factor that indicates how the specular component of the reflected wave is reduced as a result of the roughness of the surface. D is the divergence factor caused by the fact that the reflecting surface always is convex.

The grazing angle, ψ , appears at the point of reflection between the beam and the tangent to the surface, see Fig. 9. This angle is used when calculating the

reflection factor and found by analysis of the relations in Fig. 9 as

$$\psi \cong \sin^{-1} \left(\frac{H_T}{R_1} - \frac{R_1}{2R_e} \right). \quad (20)$$

Further, it is possible to calculate ρ_0 as

$$\rho_0 = \frac{\sin(\psi) - \sqrt{\varepsilon_c - \cos^2(\psi)}}{\sin(\psi) + \sqrt{\varepsilon_c - \cos^2(\psi)}} \quad (21)$$

where

$$\varepsilon_c = \varepsilon_r - j\varepsilon_i = \varepsilon_r - j60\lambda_r\sigma_e \quad (22)$$

and ε_r is the ordinary dielectric constant, λ_r is wavelength in meters and σ_e is the conductivity in mhos/m. ρ_s is then derived from

$$\rho_s = e^{-z} I_0(z) \quad (23)$$

where I_0 denotes the modified Bessel function of zero order and

$$z = 2 \left(\frac{2\pi\sigma_h \sin(\psi)}{\lambda} \right). \quad (24)$$

Here, σ_h is the standard deviation, STD, of the amplitude distribution of the sea waves and ρ_s is valid on the interval $0 \leq \frac{\rho_s \sin(\psi)}{\lambda} \leq 0.3$.

The sea state, *ss*, is an index for STD of the sea wave altitudes, σ_h , and calculated from [8].

Table 1
STD OF SEA WAVE ALTITUDES FOR DIFFERENT SEA STATES

Sea state, <i>ss</i>	σ_h [m]
1	0.05
2	0.15
3	0.30
4	0.50
5	0.75

In Table 1 different ss indicates what STD that is used in meters.

Due to that the point where the reflection occur always is curved (convex) rather than flat, this means that the curvature of the reflected wave front will be different from the incident wave, which affects the field intensity at this specific point. Therefore an divergence factor is derived as

$$D \approx \left(1 + \frac{2G_{d1}G_{d2}}{R_e G_d \sin(\psi)}\right)^{-1/2}. \quad (25)$$

This is just an adequate approximation but can according to [2] be used in all cases of interest.

2.1.1.5 Radar Model

The radar is assumed equipped with a beam changing system with fixed beam positions. When the signal is transmitted the beam always is directed horizontally, But the beam of the receiving antenna can be adjusted in elevation. Transmission and receiving is always done in pairs and the received signals angle is either up or down, the so-called up- and down beam.

The antenna diagram can be derived with [4]

$$A_k = 1 - 2\left(\frac{\theta_b}{4\lambda_r}\right)^2 \cos\left(0.81\frac{\theta_b}{\lambda_r} + k\frac{\pi}{6}\right). \quad (26)$$

Here A_k is the normalized amplitude gain factor. The index $k \in \{0, 1, -1\}$ represent the transmitted beam, received up- and down beam. θ_b is the elevation angle, where $b = \{r, d\}$ which is described in Fig. 9, and λ_r is the radar wavelength.

In order to increase the resolution in range without reducing the pulse duration, pulse compression is used. An approximated Gaussian function is used to derive an impulse response function as [4]

$$h_{pc}(r) = 10^{-0.6\left(\frac{r}{r_3}\right)^2} \quad (27)$$

where r is a vector with each sample value and r_3 the pulses 3 dB bandwidth.

The pulse compression in radar systems is implemented in the digital domain in which only a discrete-time version of the compressed pulse is obtained. Therefore the sampling points will be uncorrelated with the compressed pulses posi-

tion. Thus, the positions for maximum amplitude, continuous-time and discrete-time pulse, typically are separated by a range, r_f [4]. How r_f is defined is illustrated in Fig. 10.

2.1.2 Model on Matrix Form

The model can be formulated as

$$\mathbf{x} = \mathbf{A}(\theta)\mathbf{s} + \mathbf{n} \quad (28)$$

where \mathbf{x} is the observation vector from the received signal, $\mathbf{A}(\theta)$ a transfer matrix that particularly contains the radar geometry and properties in the reflection surface, \mathbf{s} the normalized target amplitudes, \mathbf{n} Gaussian colored noise and θ the two parameters that should be estimated. When a multipath effect occurs the resolution in angle is usually not good enough to separate the target from the multipath target. This means that the multipath target interacts with the true target and impairs the altitude measurement result [4]. Except for the angle difference of the target and multipath target they also differs in range. Compared to the angle resolution the range resolution for the radar is much better and only limited by its bandwidth. Since the range δ_R between the targets direct echo and second multipath echo contains information about the targets altitude, this is a good parameter to observe when the altitude should be estimated. Another possibility is to observe the targets altitude directly itself. θ 's search space can therefore be chosen to span over either δ_R or H_T . The other estimation parameter is chosen to be r_f , which is the deviation between sampled signal and true signal, as illustrated in Fig. 10.

If $x_u(n)$ and $x_d(n)$ are sampled values in range direction of the received signals up- and down beam. The total signal \mathbf{x} with N complex values from both beam positions can be described by

$$\mathbf{x}[\mathbf{n}] = [x_u(0) \dots x_u(N-1) \quad x_d(0) \dots x_d(N-1)]^T \quad (29)$$

Note that this can not be regarded as one continuous signal, rather a composition of two independent signals.

Due to company confidential reasons the input signal \mathbf{x} must be created, and therefore not obtained from a true radar system. In the created model the target reflectors are described of probabilities and every new pulse echo gets a new random value as mentioned in subsection 2.1.1.1.

The transfer matrix \mathbf{A} is describing the transfer from the normalized target amplitude \mathbf{s} to the received signal, \mathbf{x} [4]. This is derived as

$$\mathbf{A} = \begin{bmatrix} g_u(0) & g'_u(0) & g''_u(0) & 0 & 0 & 0 \\ \vdots & \vdots & \vdots & \vdots & \vdots & \vdots \\ g_u(N-1) & g'_u(N-1) & g''_u(N-1) & 0 & 0 & 0 \\ 0 & 0 & 0 & g_d(0) & g'_d(0) & g''_d(0) \\ \vdots & \vdots & \vdots & \vdots & \vdots & \vdots \\ 0 & 0 & 0 & g_d(N-1) & g'_d(N-1) & g''_d(N-1) \end{bmatrix} \quad (30)$$

where

$$\mathbf{g}_j(n) = G_j h_{pc}((n - n_0)r_s + r_f), \quad (31)$$

$$\mathbf{g}'_j(n) = G'_j h_{pc}((n - n_0)r_s - \frac{\delta_R}{2} + r_f)\rho, \quad (32)$$

$$\mathbf{g}''_j(n) = G''_j h_{pc}((n - n_0)r_s - \delta_R + r_f)\rho^2. \quad (33)$$

$\mathbf{g}_j(n)$, $\mathbf{g}'_j(n)$ and $\mathbf{g}''_j(n)$ is the signal characteristic for the direct, first multipath and second multipath echo, respectively. r_s is used to convert samples to meter and $j \in \{u, d\}$, representing up- and down-beam. Further,

$$G_j = A_{j,T}(\theta_d)A_{j,R}(\theta_d), \quad (34)$$

$$G'_j = A_{j,T}(\theta_d)A_{j,R}(\theta_r) + A_{j,T}(\theta_r)A_{j,R}(\theta_d), \quad (35)$$

$$G''_j = A_{j,T}(\theta_r)A_{j,R}(\theta_r) \quad (36)$$

where $A_{j,T}$ and $A_{j,R}$ are the normalized antenna gain amplitude factor at transmission and receiving, respectively.

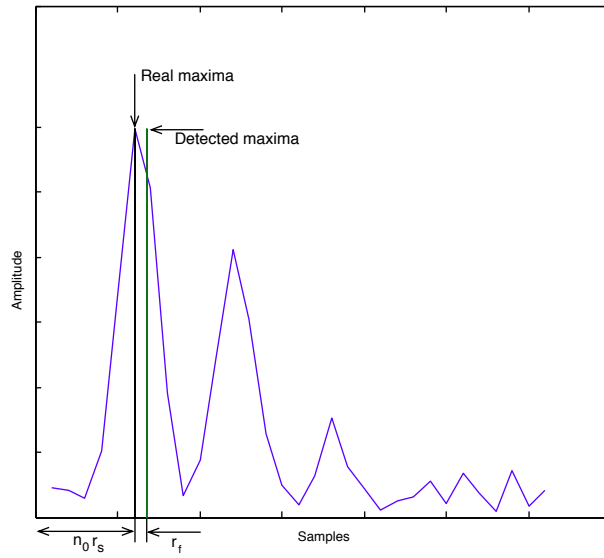


Figure 10: Input-signal \mathbf{x} for one beam with r_f , r_s and n_0 described.

Fig. 10 describes a received signal \mathbf{x} for one beam and shows how r_f , r_s and n_0 is defined. n_0 is the number of samples to the first detected peak.

The transfer matrix $\mathbf{A}(\theta)$ can be seen as a similarity of the input signal \mathbf{x} with six pulses, three for the up- and three for the down beam.

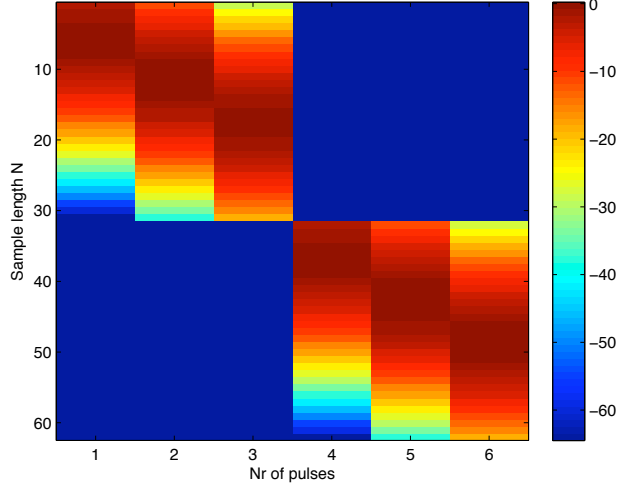


Figure 11: Example of \mathbf{A} -matrix (logarithmic, $N=31$) where the six highest values represent the six pulses peaks. Notice that the colorbar has the highest value at zero.

Fig. 11 shows an example of a logarithmic \mathbf{A} matrix with a sample length of 31 for each beam, i.e. a total of 62 samples.

2.1.3 Model Simplifications

Since the altitude measurement algorithm involves heavy calculations, some model simplifications can make a big difference. It is therefore studied if some functions can be linearized or if other knowledge about the input-signal can be taken into consideration. This is with respect to a balance between performance and computational burden.

One option for this matter is mainly to pre-calculate and store results as much as possible. A good start can be to save every possible combinations for $\mathbf{A}(\theta)$ on the selected grid in the parameter space. Like mentioned before, θ 's search space is chosen to span over either H_T and r_f or δ_R and r_f . If $\mathbf{A}(\theta)$'s each element equations are analysed, (31), (32) and (33), it can be seen that H_T is nested upstream in the equations, unlike δ_R . If data should be saved it would therefore be easier to use δ_R as an estimation parameter. This means that $\mathbf{A}(\theta)$ can be saved with different θ 's if G_j , G'_j , G''_j and ρ can be seen as scalars and the sampling range, r_s , as a constant value.

The expressions given by (34), (35), (36) and ρ are therefore saved as con-

stant scalars and r_s , is selected to always be a constant value. In subsection 3.4.1.1 the results with a Total Grid Search with saved data, TGS-s, and Total Grid Search without saved data, TGS-ns, is shown.

A further aspect, when the estimation is made over δ_R is that H_T needs to be derived afterwards. This can either be done if H_T is solved from the approximated flat Earth model (3) or the spherical Earth model (17). But to explicitly solve H_T as a function of δ_R from (17) is basically impossible. Instead, a simple function is developed where δ_R is calculated with an arbitrary number of target altitudes that are compared with the estimations of δ_R . In a mathematical way the equation to solve can be expressed by

$$\hat{\delta}_R - f(H_T, H_R, R_T) = 0 \quad (37)$$

where H_T is iteratively tested in the range between 0:0.1:30 km. \hat{H}_T is then chosen where (37) is closest to zero. To estimate H_T from δ_R is still costly in computational power and due to this fact an interpolation is implemented. By interpolating H_T in the interval from 0 to 30 km and calculate every 2 km instead of 0.1 km means a cost save. How this effect the outcome is described in subsection 3.4.2.5.

2.2 Least-Squares Estimate (LSE)

Generally LSE does not require any statistical knowledge about the observed data vector \mathbf{x} , which distinguish it from many other methods. The only requirement is that there exist a model for how the observed data \mathbf{x} depends on θ .

The LSE-loss function that should be minimized can be formulated as [6]

$$\mathbf{L}(\theta, \mathbf{s}) = \|\mathbf{x} - \mathbf{A}(\theta)\mathbf{s}\|^2. \quad (38)$$

If \mathbf{s} is seen as a linear parameter in the model it can analytically be substituted by a least-squares estimate of \mathbf{s} . From [6] it is shown that

$$\hat{\mathbf{s}} = (\mathbf{A}^T \mathbf{A})^{-1} \mathbf{A}^T \mathbf{x} \quad (39)$$

which give the concentrated LSE-loss function [7].

$$\mathbf{L}(\theta) = \|\mathbf{x} - \mathbf{A}(\mathbf{A}^T \mathbf{A})^{-1} \mathbf{A}^T \mathbf{x}\|^2 = \epsilon^T(\theta)\epsilon(\theta) \quad (40)$$

where the least-squares residual

$$\epsilon(\theta) = (\mathbf{I} - \mathbf{A}(\mathbf{A}^T \mathbf{A})^{-1} \mathbf{A}^T) \mathbf{x} = \mathbf{P}^\perp \mathbf{x} \quad (41)$$

and the matrix \mathbf{A} depend on a parameter vector θ [7]. The projection matrix

\mathbf{P}^\perp is the orthogonal projection of the complement to \mathbf{A} 's column space. As described in subsection 2.1.3, it is possible to pre-save every possible combinations for $\mathbf{A}(\theta)$, but as can be seen in (41) it is then also possible to pre-save \mathbf{P}^\perp . When \mathbf{s} is substituted with its estimate it is possible to neglect the impact of the reflection parameter ρ , and it can be applied to a constant value of one [4]. The only unknown parameters are then the nonlinear parameters in θ , which means that the final solution is to find a θ that minimizes (40).

In this specific case, \mathbf{x} is a complex vector and ϵ is complex valued. The norm in the loss function is therefore needed to be given by [7]

$$\mathbf{L}(\theta) = \|\mathbf{x} - \mathbf{A}(\mathbf{A}^T \mathbf{A})^{-1} \mathbf{A}^T \mathbf{x}\|^2 = \|\epsilon(\theta)\|^2 = \epsilon^H(\theta)\epsilon(\theta) \quad (42)$$

where $(\cdot)^H$ is the hermitian transpose, i.e. transpose and complex conjugation. According to [7], the loss function can be reformulated to

$$\mathbf{L}(\theta) = \|\epsilon(\theta)\|^2 = \epsilon^H(\theta)\epsilon(\theta) = (\text{Re } \epsilon(\theta))^2 + (\text{Im } \epsilon(\theta))^2 = \left\| \begin{bmatrix} \text{Re } \epsilon(\theta) \\ \text{Im } \epsilon(\theta) \end{bmatrix} \right\|^2. \quad (43)$$

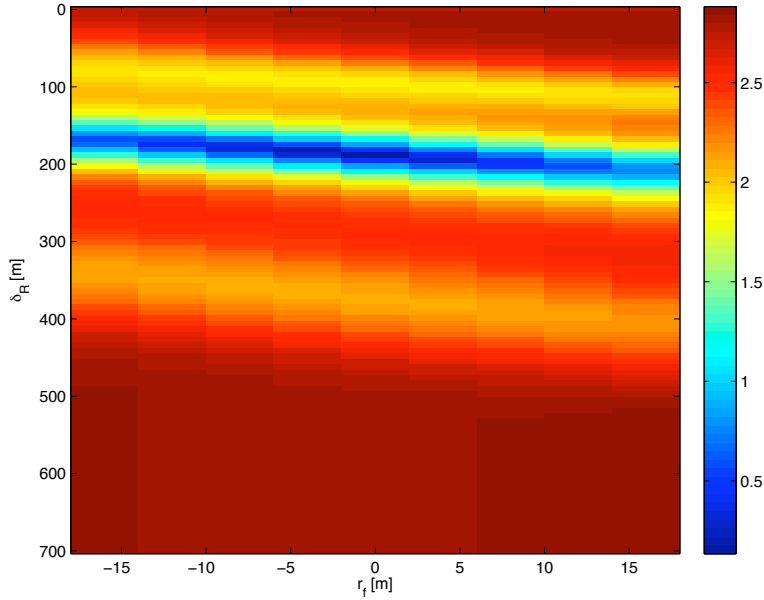


Figure 12: Loss functions plot (LSE-loss matrix) with minimum at $\delta_R = 185$ and $r_f = 0$.

Fig. 12 illustrates an example of the LSE error when the estimation parameters in θ are δ_R and r_f . The characteristic is achieved when the algorithm iteratively updates (43) with different θ . Here, $\delta_R = 185$ and $r_f = 0$ have obtained the least-squares error. The estimation space is chosen from 0:7:700 in δ_R and -16:4:16 in r_f . Notice that this will give an estimation space with 101 times 9 values.

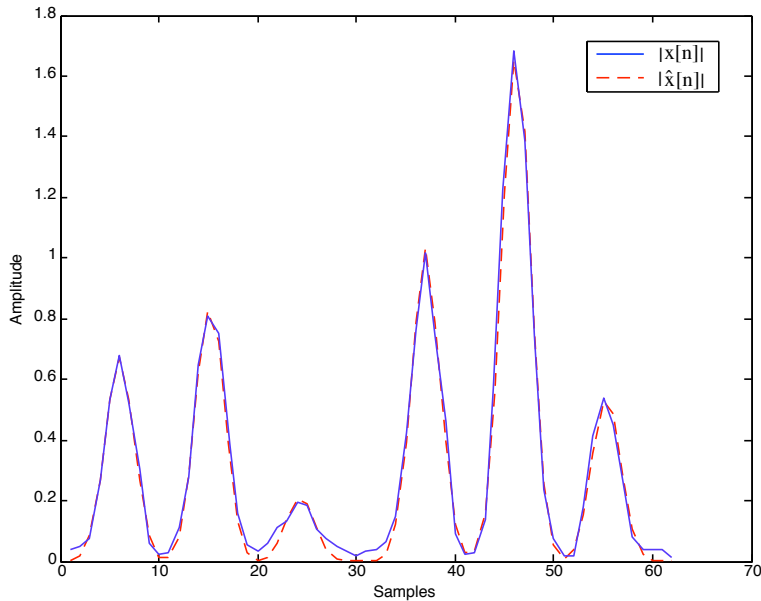


Figure 13: Plot of $|\mathbf{x}[\mathbf{n}]|$ and $|\hat{\mathbf{x}}[\mathbf{n}]|$.

In Fig. 13 it is shown how the LSE algorithm has found the best fit to the input signal \mathbf{x} . Here, $\hat{\mathbf{x}} = \mathbf{A}\hat{\mathbf{S}}$, and note how it does take both the pulses amplitude and their mutual position into consideration. The first three pulses are the up-beam and the last three pulses the down-beam, i.e. two different concatenated signals.

2.3 Numerical Search Methods

Since the estimation method LSE has been tested before, the focus of this project is to find a search method that can find its global grid minimum, which is described in this section. The objective is to find a method so that the number of iterations for the derived LSE-loss functions can be reduced. To improve understanding, the search methods are illustrated with a search in the total grid. Note that the search methods only have the knowledge of their calculated values.

2.3.1 Total Grid Search (TGS)

When the LSE-loss function is derived with different θ 's, these values are assigned to a matrix which generates a result like in Fig. 12. This means that each value for the specified estimation space is derived, i.e. each coordinate in the figure. This is called a Total Grid Search, TGS, and can always guarantee that the global grid minimum is found, but contributes to a high computational cost. Since TGS can guarantee a global grid minimum this is used as a method to evaluate LSE's performance.

2.3.2 Numerical Neighborhood Search (NN)

To reduce the number of iterations, and thereby also the computational burden, any algorithm needs to be applied where all LSE-loss values not needs to be derived. With a defined number of starting points the algorithm should search for local grid minima and converge as fast as possible to reduce the computational burden. The easiest and most simple algorithm applied in this project is the Numerical Neighborhood search, NN, This method derives the loss function value for all 8 neighbors and if one neighboring value is less than the present value, the algorithm moves there and starts over. Otherwise a local minimum on the predefined parameter grid has been found.

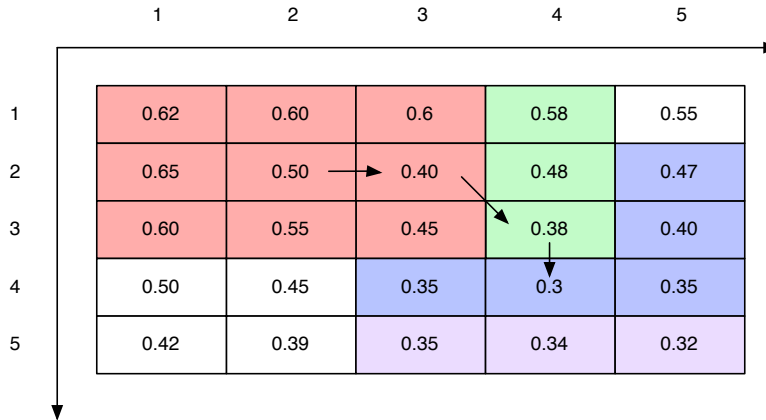


Figure 14: Description of NN iterations to a local minimum.

Fig. 14 illustrates how the NN algorithm iterates from a starting position (2,2) to its local minimum at (4,4). The different colors describes how the algorithm is optimized not to calculate a coordinates value more than ones, e.g. when (3,2) is reached only (4,1), (4,2) and (4,3) needs to be derived since the other neighbors are known.

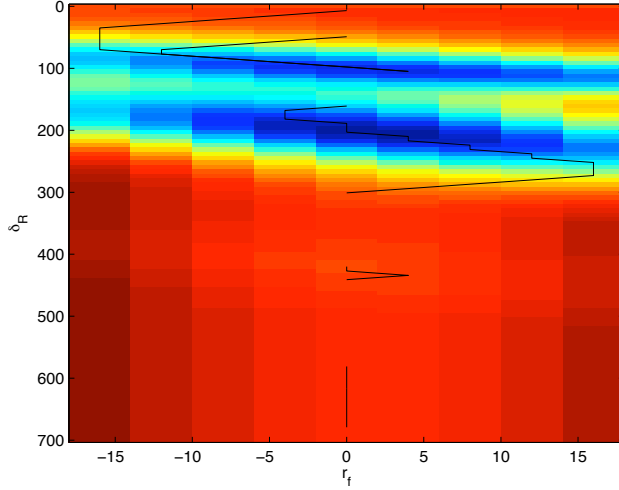


Figure 15: Typical path for NN with 7 starting points.

A typical path with seven starting points can be seen in Fig. 15.

2.3.3 Gauss Newton with Line Search (GN)

The Gauss Newton with line search, GN, algorithm is an iterative method regularly used for solving nonlinear Least-Squares problems. In comparison with Newton's methods and its variants, the GN method does not require any second-order derivatives in the Jacobian of the objective function, and therefore it has become an attractive method [3].

If the GN minimization algorithm is applied where the input signal \mathbf{x} is complex valued and

$$\mathbf{L}(\theta) = \epsilon^H(\theta)\epsilon(\theta) \quad (44)$$

should be minimized, the steps can be summarized by [7]:

Step 0: Choose an initial $\theta^m|_{m=0} \in R^n$, where n is the search space dimension and m the number of iterations.

Step 1: Derive $\epsilon(\theta^m)$ and the real-valued Jacobian \tilde{J} to get the gradient, G , of the loss function \mathbf{L} .

Step 2: If \mathbf{A} is real-valued and \mathbf{x} is complex-valued the GN search direction is derived as

$$\delta\theta = -(\tilde{\mathbf{J}}^T \tilde{\mathbf{J}})^{-1} \tilde{\mathbf{J}}^T \begin{bmatrix} \mathbf{P}^\perp \text{Re } \mathbf{x} \\ \mathbf{P}^\perp \text{Im } \mathbf{x} \end{bmatrix} = -(\tilde{\mathbf{J}}^T \tilde{\mathbf{J}})^{-1} \tilde{\mathbf{J}}^T \begin{bmatrix} \text{Re } \epsilon(\theta) \\ \text{Im } \epsilon(\theta) \end{bmatrix}. \quad (45)$$

Step 3: Make a line search controlled by the magnitude of the gradient

$$\min_{\alpha} \mathbf{L}(\theta^m + \alpha\delta\theta). \quad (46)$$

Step 4: Check for convergence

$$\frac{\|\alpha\delta\theta\|^2}{\|\theta^m\|^2} < \theta_{\text{lim}} \quad \text{or} \quad \frac{\mathbf{L}(\theta^m) - \mathbf{L}(\theta^m + \alpha\delta\theta)}{\mathbf{L}(\theta^m)} < \mathbf{L}_{\text{lim}} \quad \text{or} \quad m > m_{\text{max}}. \quad (47)$$

Step 5: If no convergence criteria is satisfied

$$\theta^{m+1} = \theta^m + \alpha\delta\theta, \quad m = m + 1 \quad (48)$$

and go to step 1. Otherwise,

$$\theta_{\text{opt}} = \theta^m + \alpha\delta\theta. \quad (49)$$

The gradient of the loss function \mathbf{L} is given by [7]

$$\mathbf{G} = \frac{\partial \mathbf{L}(\theta)}{\partial \theta} = \tilde{\mathbf{J}}^T \begin{bmatrix} \text{Re } \epsilon(\theta) \\ \text{Im } \epsilon(\theta) \end{bmatrix} \quad (50)$$

where

$$\tilde{\mathbf{J}} = \begin{bmatrix} \text{Re } \mathbf{J} \\ \text{Im } \mathbf{J} \end{bmatrix} \quad (51)$$

and

$$\text{Re } \mathbf{J} = [(\frac{\partial}{\partial \theta_1} \mathbf{P}^\perp) \text{Re } \mathbf{x}, (\frac{\partial}{\partial \theta_2} \mathbf{P}^\perp) \text{Re } \mathbf{x}, \dots, (\frac{\partial}{\partial \theta_n} \mathbf{P}^\perp) \text{Re } \mathbf{x}], \quad (52)$$

$$\text{Im } \mathbf{J} = [(\frac{\partial}{\partial \theta_1} \mathbf{P}^\perp) \text{Im } \mathbf{x}, (\frac{\partial}{\partial \theta_2} \mathbf{P}^\perp) \text{Im } \mathbf{x}, \dots, (\frac{\partial}{\partial \theta_n} \mathbf{P}^\perp) \text{Im } \mathbf{x}]. \quad (53)$$

Further, $\frac{\partial}{\partial \theta} \mathbf{P}^\perp$, needs to be calculated. If

$$\mathbf{P}^\perp = (I - (\mathbf{A}^T \mathbf{A})^{-1} \mathbf{A}^T) \quad (54)$$

and

$$\dot{\mathbf{A}} = \frac{\partial \mathbf{A}}{\partial \theta} \quad (55)$$

is defined, the following formula can be derived with the product and inverse rule as [7]

$$\frac{\partial}{\partial \theta} \mathbf{P}^\perp = -\dot{\mathbf{A}}(\mathbf{A}^T \mathbf{A})^{-1} \mathbf{A}^T - \mathbf{A}(\mathbf{A}^T \mathbf{A})^{-1} \dot{\mathbf{A}}^T + \mathbf{A}(\mathbf{A}^T \mathbf{A})^{-1} (\mathbf{A}^T \dot{\mathbf{A}} + \dot{\mathbf{A}}^T \mathbf{A}) (\mathbf{A}^T \mathbf{A})^{-1} \mathbf{A}^T. \quad (56)$$

When this is implemented for step 1 in the summarized steps, an entire GN sequence can be performed to find a local minimum θ_{opt} . As described in subsection 2.1.3, it is allowed to save data to reduce the computational burden. When a GN search is performed, $\frac{\partial}{\partial \theta} \mathbf{P}^\perp$ needs to be derived for each iteration. Instead of doing this it is possible to pre-save all these values in a matrix, which is advantageous if the computational burden should be reduced with GN. A typical path with 7 starting points for the algorithm can be illustrated as

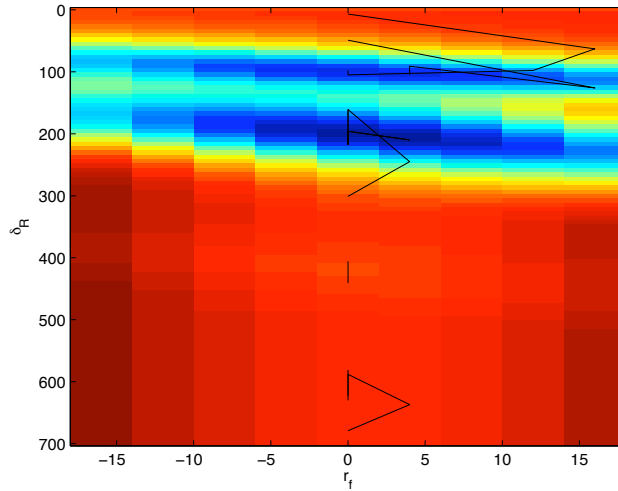


Figure 16: Typical path for GN with 7 starting points.

2.3.4 Steepest Descent with Line Search (SD)

Since the computational burden would be extremely heavy when calculating $\frac{\partial}{\partial \theta} \mathbf{P}^\perp$ for every iteration in a GN sequence it is required that both \mathbf{P}^\perp and $\frac{\partial}{\partial \theta} \mathbf{P}^\perp$ is pre-saved. A solution to avoid that $\frac{\partial}{\partial \theta} \mathbf{P}^\perp$ needs to be used is if the derivative of the loss function \mathbf{L} is approximated to

$$\frac{\partial \mathbf{L}(\theta)}{\partial \theta} \approx \frac{\mathbf{L}(\theta + \delta\theta) - \mathbf{L}(\theta)}{\delta\theta}. \quad (57)$$

The difference between this method and GN is that the gradient for a new search direction is approximated instead of derived analytical, and is called a Steepest Descent with line search, SD. This will only require that \mathbf{P}^\perp is pre-saved.

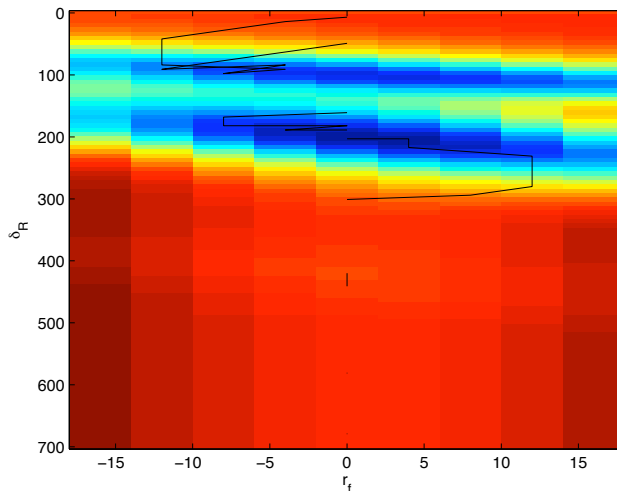


Figure 17: Typical path for SD with 7 starting points.

Fig. 17 illustrates a typical path for SD with 7 starting points.

2.3.5 GN with NN

When a GN step is derived this gives a new grid coordinate in parameter space. However, since the search is performed on a fixed parameter grid the new coordinate needs to be truncated to a grid point. This process leads to that the GN method is not guaranteed to converge to the local optimum on the defined grid. This means that a finer grid will obtain better estimates. But a finer grid search will increase the required pre-saved data significantly. Instead a final NN search is applied at the end of every GN convergence point, so that a local minimum can be guaranteed.

2.3.6 Number of Starting Points

Yet, it is not discussed how the starting points are selected, which is a crucial step for each search method. The more starting points that are generated the higher is the probability that the global minimum is found. If only one starting

point is generated it is likely that only a local minimum is found. Like in general optimization problems there have to be a balance between computational burden and performance.

By only analyse different LSE-loss matrices a recurrent behavior is that most minima are located in the middle of the r_f -axis. The starting points are therefore chosen to start at $r_f = 0$. The number of starting points, their mutual position and the LSE-loss matrices are then varied to find a point of convergence. One contradictory aspect with this test is that the result depends on how the minima are placed in the matrices. If the targets altitude for a test case is fixed, all global minima might be placed at the same place, and therefore, it does not always give better results with more starting points.

2.4 General Extensions

In addition to the different search methods, some general extensions and theories are considered.

2.4.1 Median of Several Estimations

Earlier in the report, every input signal is seen as a shared setting of one up- and one down beam, but for an entire search mode there are not only one signal to analyse. Actually this is done several times which means that much more information about one target can be collected. Therefore a final median value for an altitude measurement of the estimations is collected.

2.4.2 Quality Index

To get an idea of how good every single estimation is, a quality index, QI, is calculated for each measurement. One way of evaluate a QI is with knowledge about the LSE-loss matrix and the found global grid minimum, as in a TGS. If the global solution has a big deviation from the mean of every derived LSE-loss value, the estimation is assumed to be good and a high QI is assigned. Vice versa, when the deviation is small a low QI is assigned. The QI is derived by

$$QI = |\overline{\mathbf{L}(\theta)} - \mathbf{L}(\theta_{\mathbf{gmin}})| \quad (58)$$

where $\overline{\mathbf{L}}$ represent the mean of every derived LSE-loss value and $\mathbf{L}(\theta_{\mathbf{gmin}})$ the lowest LSE-loss value found.

For the optimization methods and algorithms, knowledge about the total LSE-loss matrix, $\overline{\mathbf{L}}$, is missed. Instead the two lowest local minima found can be taken into account. A QI is instead derived by

$$QI = \|\mathbf{x}\|^2 - \mathbf{L}(\theta_{\mathbf{gmin}}) \cdot \frac{\mathbf{L}(\theta_{\mathbf{gmin}}) - \mathbf{L}(\theta_{\mathbf{lmin}})}{\mathbf{L}(\theta_{\mathbf{gmin}})}, \quad (59)$$

where $\bar{\mathbf{L}}$ is replaced with $\|\mathbf{x}\|^2$ and the second lowest minimum found $\mathbf{L}(\theta_{\mathbf{lmin}})$ are considered. $\|\mathbf{x}\|^2$ can be seen as the energy in the input signal, \mathbf{x} , and is an estimation of the total loss-function $\|\mathbf{x} - \hat{\mathbf{s}}\|^2$.

2.4.3 Performance of Pulse Separation and Signal to Noise Ratio

To identify a performance with respect to noise and resolution of δ_R , one input signal with fixed amplitudes are created.

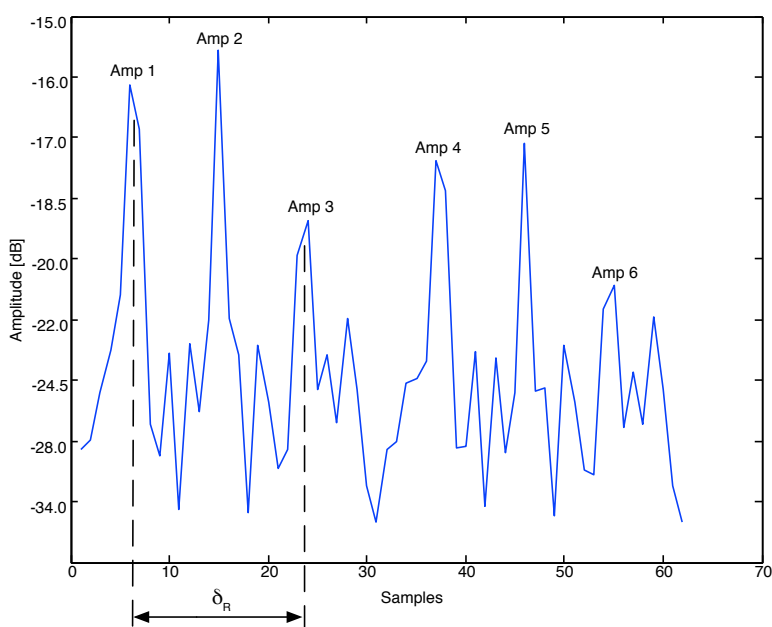


Figure 18: Illustrates a case where δ_R and SNR is changed to identify performance.

With the first amplitude, Amp1, as index, the six pulses individual amplitudes can be seen as; 0, 0.9, -2.3, -0.9, -0.6 and -4.3 illustrated in Fig. 18. Instead of compare different noise levels the Signal to Noise Ratio, SNR is used and derived by

$$SNR = \frac{a^2}{\text{var}(\mathbf{n})}, \quad (60)$$

Where a is the pulses amplitude and \mathbf{n} Gaussian colored noise. (60) describes how SNR can be derived, which is explained as the level between noise and the pulses amplitude. The SNR is calculated for Amp1 and Amp4 in Fig. 18

and then the mean of these is used. By reducing the range δ_R towards zero it is possible to detect when the algorithm not is able to resolve the multipath echoes for different SNR. When changing the range δ_R and SNR repeatedly a normed bias error and variance can be derived. This is done 100 times for 43 different δ_R and 4 different SNR. To imitate reality as good as possible every phase contribution between amplitude 1 and 4, 2 and 5, and 3 and 6 respectively is changed randomly for each signal realization.

2.4.4 Computational Burden

It is of highest interest to see how the computational burden is affected when applying the optimization search methods. To show that, in a more scientific way than time, floating-point operations (or flops²) are used. This gives an accurate and correct measure of the computational performance and is easy to use in MATLAB. Time will also be presented because it can be of interest to get a hint about the performance of the compared algorithms. The simulations are performed by a standard laptop from 2009, and all results are collected for runs with a computer of that performance.

²The function FLOPS() in MATLAB is removed in version 6 onwards. When producing the result in flops version 5 of MATLAB is used.

3 RESULTS

Results are produced with the LSE method and subsequently search algorithms are applied. The outcome of this is that a comparison between the computational burden and performance can be accomplished.

3.1 Creation of Input Signal

To present the performance and improvements a created input signal, \mathbf{x} , is used. This is because of company confidential information, and only a few results are derived with true recorded radar signals.

Table 2
PARAMETERS FOR THE RADAR SCENARIOS STUDIED

R_T [km]	H_T [km]	SNR [dB]	ss	N	H_R [km]
251:4:450	10.2,7.2,5.2,3.2	27,22,17,12	3	31	6

When the created scenario is implemented the parameters are chosen as in Table 2.

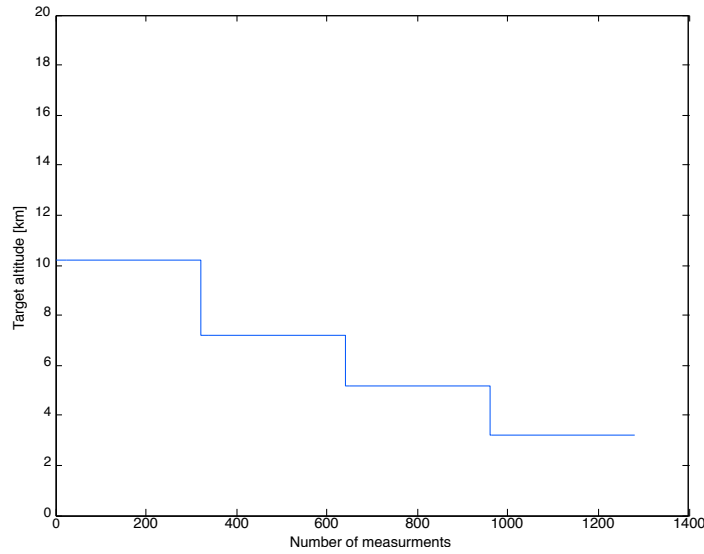


Figure 19: Targets altitude path for the created input signal.

The scenario can be explained as in Fig. 19 by a target moving away while it drops in altitude, i.e. R_T is increasing and H_T decreasing. The altitude of the

radar, H_R , is fixed to 6 km. A result of this is that the range between the pulses, δ_R will decrease. To increase the variance and to put additional stress on the algorithms further, sea state, ss , is chosen to 3 and the scenario is tested with different SNR from 27 to 12 dB. All the created data has Gaussian noise colored by the receiving filter.

3.2 Calculation of Target Altitude from δ_R

As mentioned a approximated equation of calculating δ_R is

$$\delta_R = \frac{2H_R H_T}{R_T} \quad (61)$$

where assumptions of a flat Earth is considered instead of the more advanced

$$\delta_R = \frac{4 \left(H_R + \frac{H_R^2 - R_1^2}{2R_e} \right) \left(H_T + \frac{H_T^2 - R_2^2}{2R_e} \right)}{R_1 + R_2 + R_T} \quad (62)$$

where the geometric parameters arising when a spherical Earth is used. Note that both R_1 and R_2 contains highly nested expressions of H_T that makes it hard to explicitly solve H_T . When the latter is considered (37) is used iteratively to derive the estimation of H_T , with or without interpolation as described in subsection 2.1.3. This is of course more time consuming than apply the approximation of H_T , which trivial can be rewritten from (61) as

$$H_T = \frac{\delta_R R_T}{2H_R} \quad (63)$$

When the geometrical parameters are not taken into account a drift occurs in the sequence. By multiply equation (63) with a factor means that either the close range values will be correct or the ones with a target far away.

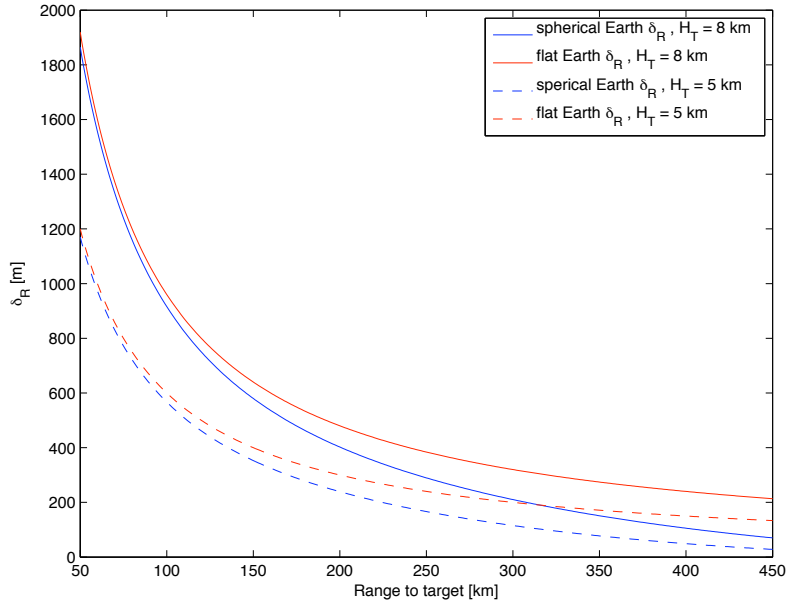


Figure 20: Differences between geometrical and non geometrical calculation of target altitude.

The simplified estimated H_T is therefore rejected and instead the function with impact of geometric parameters and spherical Earth is used. In Fig. 20 the differences of calculating target altitude for the two cases is illustrated.

3.3 Number of Starting Points Analysis

It is of interest to see how the optimization numerical search methods performance is depending of how many starting points that is generated. An analysis is therefore made where the results for GN with different starting points are compared with the global grid minimum for a TGS. The starting points are selected as

Table 3
POSITIONS FOR DIFFERENT NUMBER OF STARTING POINTS

Nr Starting Points	Positions
1	50
2	25, 75
3	25, 50, 75
4	20, 40, 60, 80
5	10, 30, 50, 70, 90
6	5, 20, 35, 55, 70, 90
7	2, 15, 30, 45, 60, 75, 90
8	2, 15, 30, 40, 50, 75, 80, 99
9	2, 10, 20, 30, 45, 55, 75, 80, 99

When increasing the number of starting points the deviation between GN with NN and TGS-s will converge towards zero.

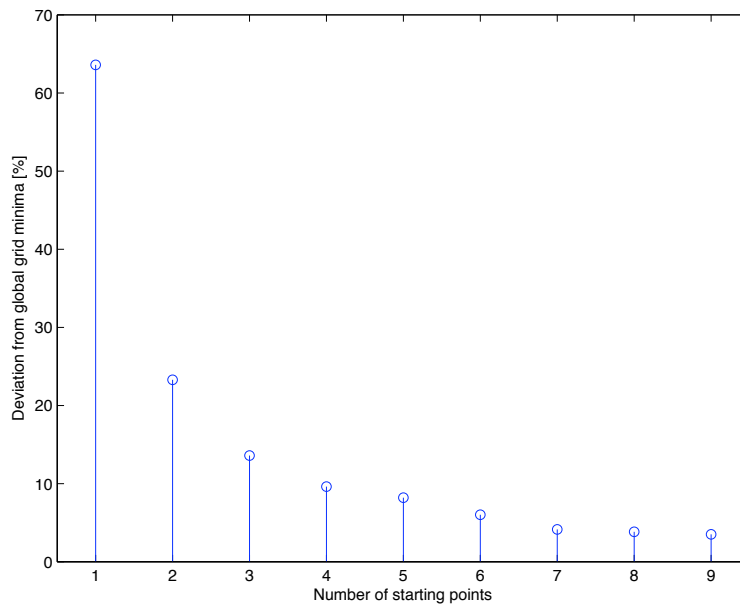


Figure 21: Illustrates the change in deviation between GN with NN and TGS-s with different number of starting points.

After 7 starting points the deviation will converge very slow which can be seen in Fig. 21, where 9 starting points is tested. 7 starting points are hereafter used

for all results where optimization algorithms are implemented.

3.4 Numerical Search Methods

This section shows the result for the different search methods. First the results for a TGS are shown and then all methods are compared to each other. The TGS is treated differently since this is the only method that can guarantee a global grid minimum and can be seen as an evaluation method for LSE.

3.4.1 Total Grid Search (TGS)

This subsection shows the performance of TGS in a case with 1280 sampled data signals.

3.4.1.1 Comparison of Simplified- and Non-Simplified TGS with True Recorded Radar Signals

First and foremost, a comparison between the simplified Total Grid Search, TGS-s, described in subsection 2.1.3 Model Simplifications, and the non-simplified Total Grid Search, TGS-ns, is shown.

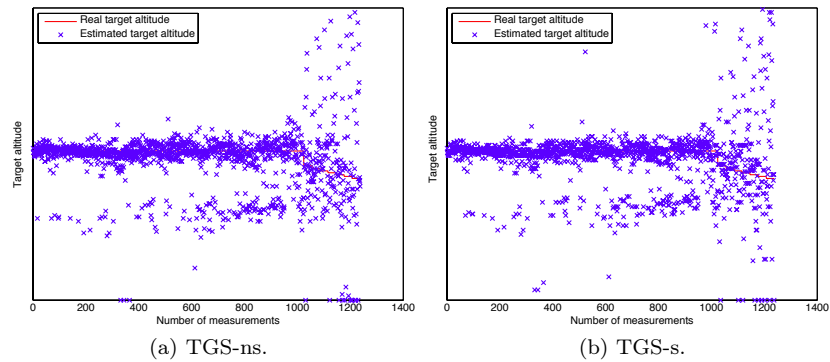


Figure 22: Altitude estimate for TGS-ns and TGS-s compared to true altitude derived with true recorded radar input signals.

Fig. 22 illustrates a non simplified- and simplified TGS altitude measurement. The scenario is derived with true recorded radar input signals and because of company confidential reasons the actual target altitude is not shown. It can still be seen that the deviation is small and the average computational time is reduced 108 times with saved data compared to non simplified case as can be seen in Table 5. Hereafter the results will therefore be represented with the simplified model.

3.4.1.2 Interaction Between SNR and δ_R

To measure the interaction between SNR and δ_R a test scenario as described in subsection 2.4.3 is done, i.e. when δ_R is decreasing for different SNR.

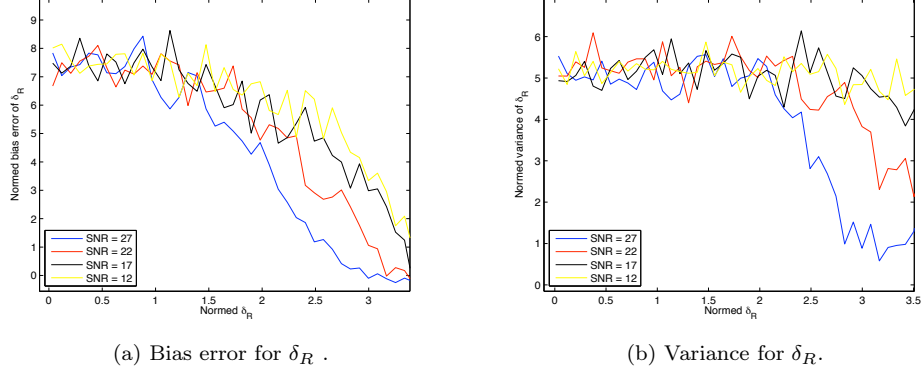


Figure 23: Bias error and variance for δ_R

To get a measure of this the bias error and variance are derived for an entire scenario which is described in Fig. 23. These results are rough estimates, and gives only an idea of the LSE performance.

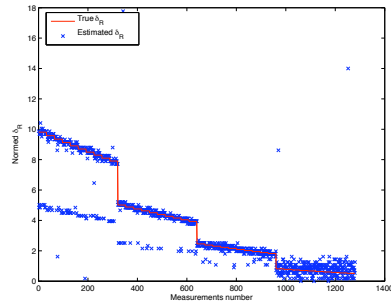
$$Bias\ error = \frac{\sum_{i=1}^{100} (\delta_{R_{est}}(i) - \delta_{R_{true}})}{n} \cdot r_3^{-1} \quad (64)$$

$$Var = \sqrt{\frac{\sum_{i=1}^{100} (\delta_{R_{est}}(i) - \delta_{R_{true}})^2}{n - 1}} \cdot r_3^{-1} \quad (65)$$

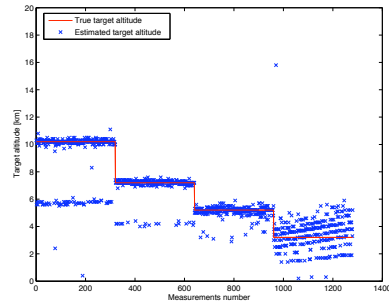
The expressions given by (64) and (65) are describing how the bias error and variance are derived when they are normed with r_3 .

3.4.1.3 Performance with Different SNR

In this subsection it is illustrated how the performance for TGS-s depends on the SNR level. The (a) figures are a comparison in δ_R and (b) a comparison in H_T after it is derived with (37).

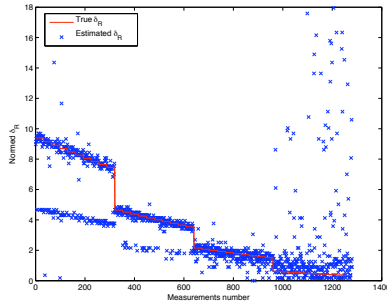


(a) Estimated δ_R compared to true δ_R .

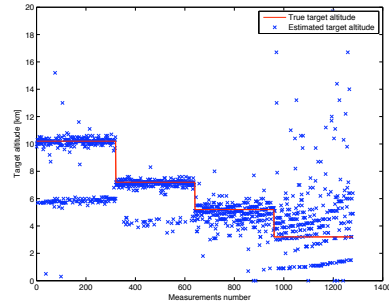


(b) Estimated H_T compared to true target altitude.

Figure 24: TGS-s compared to true altitude and δ_R with SNR = 27 dB.

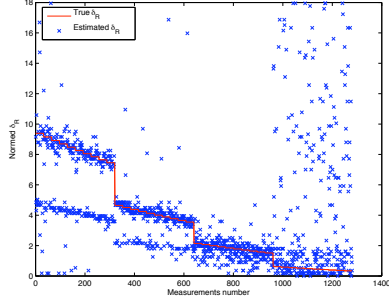


(a) Estimated δ_R compared to true δ_R .

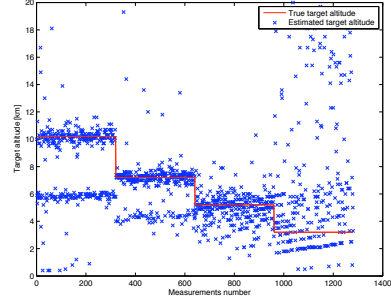


(b) Estimated H_T compared to true target altitude.

Figure 25: TGS-s compared to true altitude and δ_R with SNR = 22 dB.

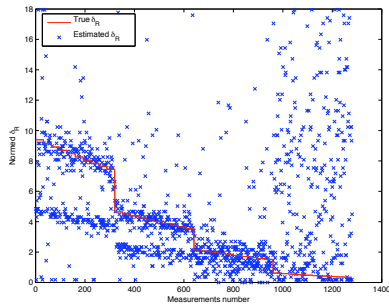


(a) Estimated δ_R compared to true δ_R .

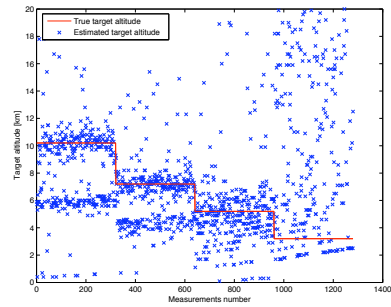


(b) Estimated H_T compared to true target altitude.

Figure 26: TGS-s compared to true altitude and δ_R with SNR = 17 dB.



(a) Estimated δ_R compared to true δ_R .



(b) Estimated H_T compared to true target altitude.

Figure 27: TGS-s compared to true altitude and δ_R with SNR = 12 dB.

In Fig. 24 to 27, results are shown where always the global grid minimum in the LSE-loss matrix are collected and compared to the true altitude. One can also see how different SNR effect the outcome.

3.4.1.4 Performance with 32 Median Measurements

When each altitude from Fig. 25, with 22 dB SNR, is divided in groups of 32 and the median of these values are calculated, a more reliable altitude measurement can be obtained.

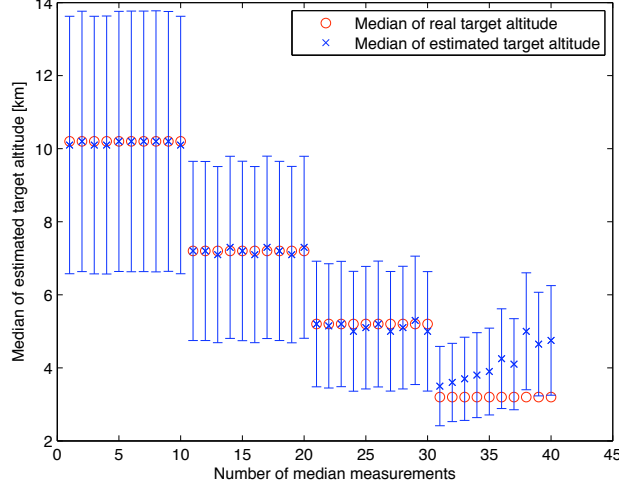


Figure 28: TGS-s compared to true altitude with median and 97,5 % confidence interval, assuming normal distribution.

The new performance with grouped values can be seen in Fig. 28. The STD with some arbitrary confidence interval for the altitude measurements is derived with [9]

$$m_{H_T} \pm \frac{t_p \cdot s_{H_T}}{\sqrt{nr}} \quad (66)$$

where s_{H_T} is the observed standard deviation for the altitude, nr is number of measurements, t_p is obtained from the t-distributed table with 30 degrees of freedom and m_{H_T} is the median of the altitude measurements. s_{H_T} is derived by [9]

$$s_{H_T} = \sqrt{\frac{1}{nr-1} \sum (H_{T_i} - m_{H_T})^2}. \quad (67)$$

The confidence interval is chosen to 97.5 % and a normal distribution is assumed.

3.4.1.5 Overview of Results for TGS-s

Table 4
OVERVIEW OF RESULTS FOR TGS-s

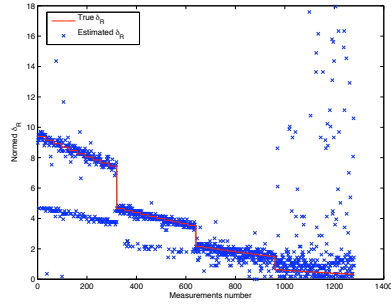
Method	Time [ms]	Flops	STD [km]		Space [MB]
			Individual	Median	
TGS-s	34.5	$2.2804 \cdot 10^7$	1.46	0.23	30.7

The computational power required and STD for TGS-s compared to true altitude are collected in Table 4. The STD individual is derived from Fig. 25 and STD median from Fig. 28. The space column illustrates the allocated space needed to store the pre-calculated P^\perp . Time is the mean time required for 1280 measurements.

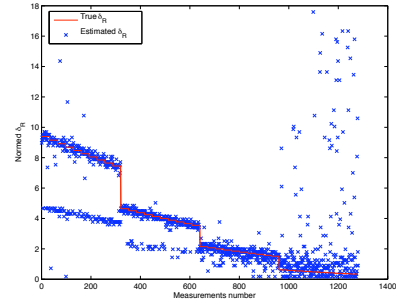
3.4.2 Comparison of Different Search Methods

In this subsection all methods are summarized and compared to each other. For these cases SNR is chosen to 22 dB. The first scenario is a comparison between true δ_R and estimated δ_R with 1280 measurements, the second and third scenario is a comparison between true H_T and estimated H_T derived from (37), with 1280 and a group of 32 median measurements, respectively. At last the deviation between the optimization search methods and TGS-s is illustrated. For the optimization methods which require starting points, seven equally distributed points are used.

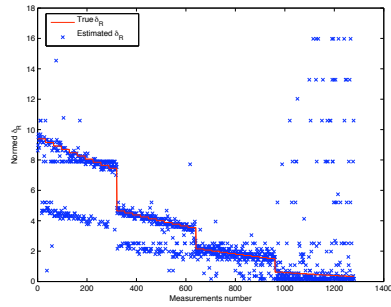
3.4.2.1 Estimated δ_R Compared with True δ_R



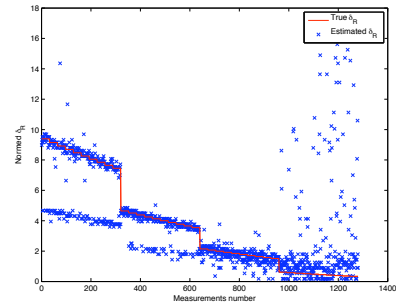
(a) TGS-s.



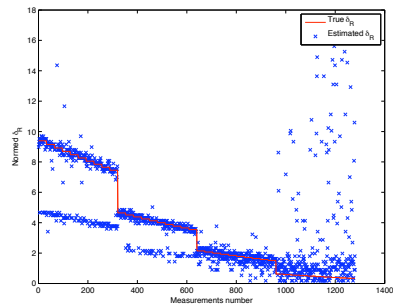
(b) NN.



(c) SD.



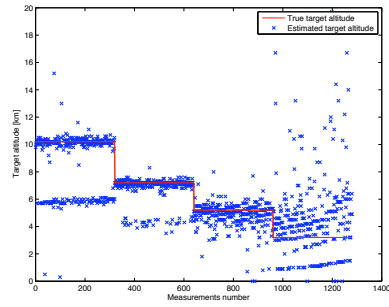
(d) GN.



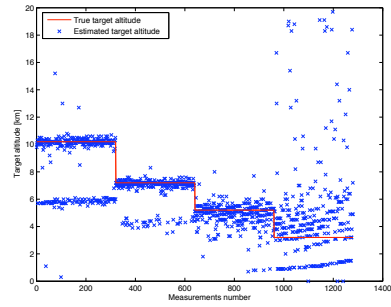
(e) GN with NN.

Figure 29: Estimated δ_R for all search methods compared with true δ_R using SNR = 22 dB.

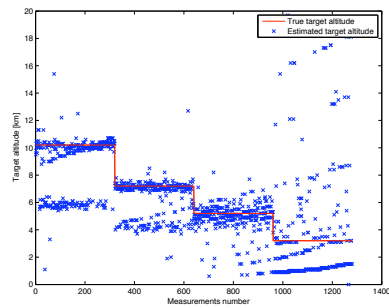
3.4.2.2 Estimated H_T Compared with True H_T



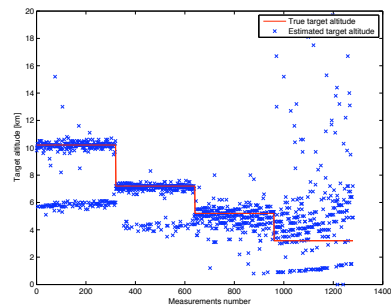
(a) TGS-s.



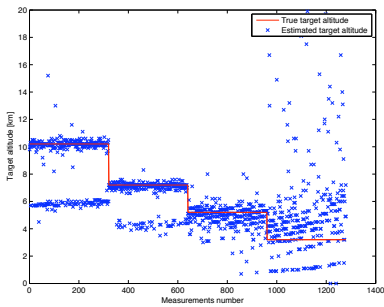
(b) NN.



(c) SD.



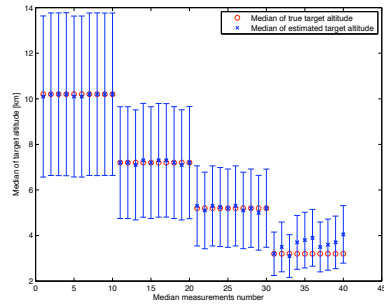
(d) GN.



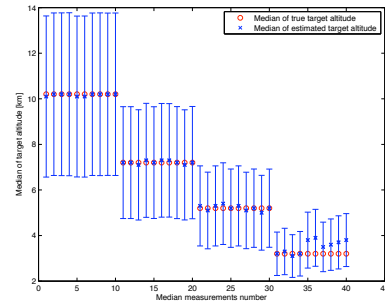
(e) GN with NN.

Figure 30: Estimated H_T for all search methods compared with true H_T using $\text{SNR} = 22$ dB.

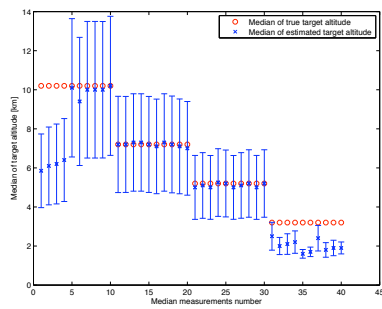
3.4.2.3 Estimated H_T Compared with True H_T using Median of 32 Measurements



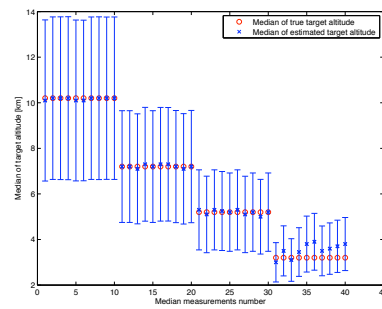
(a) TGS-s.



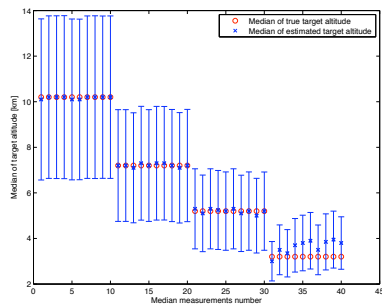
(b) NN.



(c) SD.



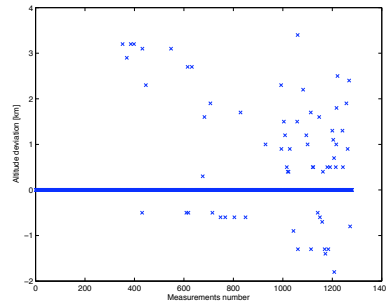
(d) GN.



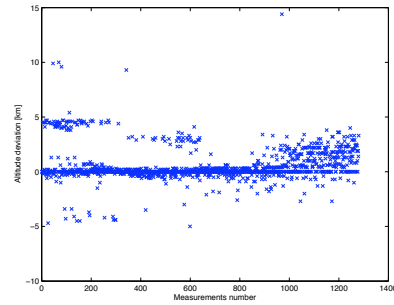
(e) GN with NN.

Figure 31: All search methods compared to true altitude with median of 32 altitude measurements. For each method a confidence interval of 97.5 % is used.

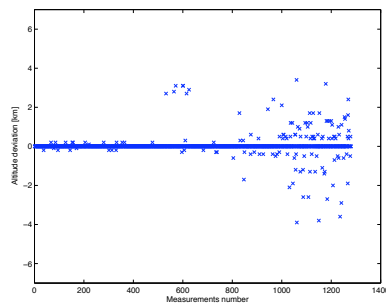
3.4.2.4 *Difference Between TGS-s and the Optimization Search Methods*



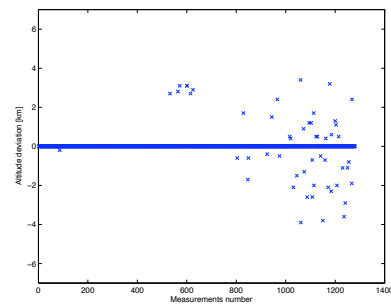
(a) TGS-s compared to NN.



(b) TGS-s compared to SD.



(c) TGS-s compared to GN.



(d) TGS-s compared to GN with NN.

Figure 32: Difference between TGS-s and the optimization search methods

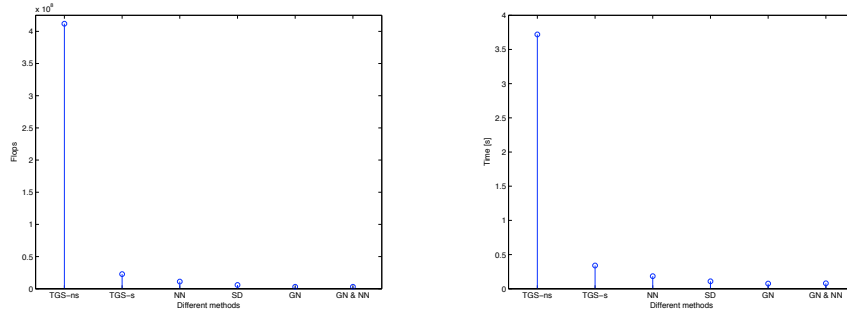
When the TGS-s is compared to the other search methods it can be seen if the methods have found the global minimum or not. Notice that TGS-s is the only method that can guarantee a global minimum. As can be seen in Fig 32 the deviation is often zero for all methods, except for SD. If the deviation is zero it means that the global grid minimum is found.

3.4.2.5 Summary of Results

Table 5
SUMMARY OF EACH METHOD

Method	Time [ms]	Flops	Perf [%]	STD [km]		Space [MB]
				Individual	Median	
TGS-ns	3720.0	$4.1193 \cdot 10^9$	-	1.51	0.23	0
TGS-s	34.5	$2.2804 \cdot 10^7$	100	1.46	0.23	30.7
NN	20.3	$1.1193 \cdot 10^7$	96.9	1.47	0.21	30.7
SD	11.8	$5.8907 \cdot 10^6$	38.2	1.66	1.23	30.7
GN	8.6	$3.1220 \cdot 10^6$	80	1.48	0.22	86.6
GN w NN	9.0	$3.1229 \cdot 10^6$	94.6	1.47	0.22	86.6

In Table 5 all search methods results are summarized. The performance represents how many of the global minima that are found, the STD is derived with respect to true altitude, H_T , where the first value is for a entire search with 1280 measurements and the second with 32 median measurements. Space means the space needed to allocate the required matrices and Time is the mean time derived from all 1280 measurements. The computational burden can also be represented visually as



(a) Flops.

(b) Mean time.

Figure 33: Summarized computational burden for the different methods visually. One can see how the computational complexity is directly related to mean time. Notice the factor for the vertical axis in the left graph (a).

Interpolation of Altitude

When calculating H_T from estimated δ_R a large influence on the total computational burden arises when (37) is tested in the range between 0:0.1:30 km. By using interpolation instead with an arbitrary number of target altitudes, a further reduction of the computational burden can be accomplished. When interpolation is used only a few values of H_T needs to be calculated, as it revealed to be similar to a linear function.

Table 6
SUMMARY OF RESULTS WHEN INTERPOLATION IS IMPLEMENTED

Method	Time [ms]	Flops	Perf [%]	STD [km]	Space [MB]
				Individual/Median	
TGS-s	34.0	$2.2780 \cdot 10^7$	100	1.48/0.22	30.7
NN	18.4	$1.1169 \cdot 10^7$	94.9	1.49/0.19	30.7
SD	10.9	$5.8668 \cdot 10^6$	40.2	1.72/1.30	30.7
GN	7.6	$3.0981 \cdot 10^6$	89.2	1.50/0.20	86.6
GN w NN	7.9	$3.0999 \cdot 10^6$	95.9	1.49/0.23	86.6

Table 6 shows the same result as in Table 5 but with interpolation implemented. The estimated H_T is interpolated in the interval from 0 to 30 km, and instead of calculate every 0.1 km only each 2 km needs to be derived as described in 2.1.3 Model Simplifications. To get an idea of what the results mean the deviation of resolution in angle can be measured. If the results for STD with median values between 1.3 to 0.19 km at a target range of 450 km were considered, this would mean a deviation from 0.16° to 0.02° in angel, which can be derived with simple trigonometry.

3.5 Quality Index (QI)

To give a hint about the quality of each measurement, a QI is calculated and presented as described in subsection 2.4.2.

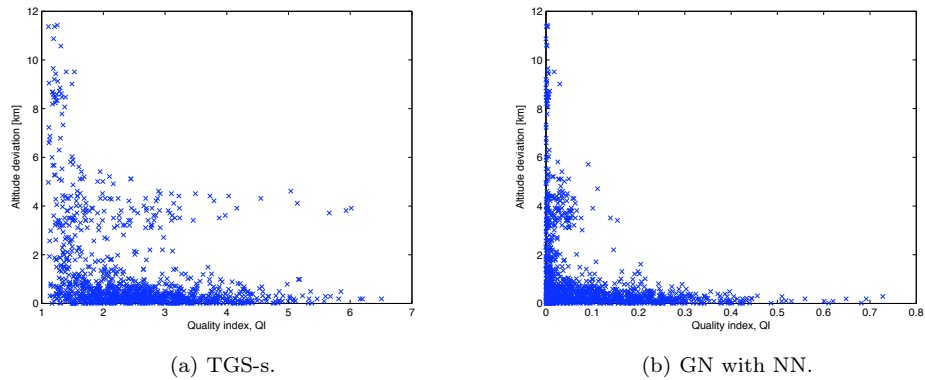


Figure 34: QI for TGS-s and GN with NN. The x-axis describes QI and y-axis the deviation from correct H_T .

The QI for TGS-s can be defined as a deviation between the LSE-loss matrix mean value and it's global grid minimum. For the optimization search methods, in addition, a deviation between the lowest and second lowest calculated LSE-loss value are considered. The result is illustrated in Fig. 34.

4 DISCUSSION

When an altitude measurement method would be used in a true radar system there are two main areas that are considered; Performance compared to computational burden and a reliability index in terms of a quality for each measurement. Something very useful is the knowledge of how much the pulses can interact compared to the SNR. Due to the infinite number of combinations for the input signals characteristic, only one typical signal is analysed for this matter. To get a perception on how reliable the measurements are, a quality index is implemented. With the implemented index it is however nearly impossible to determine if the measurement quality is poor or not. When it is possible to include the effects of multiple minima values, anyhow, it can be ensured that all the high-quality indexes have produced good estimation results. The impacts of multiple minima values are however only possible to consider when the optimization algorithms are used, which suggests these methods for this matter. With this knowledge compared to the environmental conditions, it is desired to give a better way of verify the altitude measurement performance.

When the estimated results are compared to the actual altitude, a pattern is seen where the inaccurate estimates often are half of the true altitude. This occurs when the noise level between the pulses of the input signal, \mathbf{x} , contributing to high amplitudes. Noise level has since been seen as one of the multipath pulses and the algorithm thinks the signal is more compressed than it truly is. If this somehow could be improved has not been observed, but the 32 median measurements will suppress these problems significantly.

As explained earlier in the report it is quite hard to decide an optimal number of starting points for the optimization algorithms. This is because a convergence quantity depends on how the local minima are placed. Off course the quantity can be optimized for this test case but will not be if the local minima are relocated. The starting points are therefore placed even distributed over the possible estimated altitudes. The quantity has been chosen to 7 but is a subject that must be determined after an implementation is done in a true radar system.

When an optimization algorithm is used where a gradient should be derived, such as GN, a non-square coarse grid cannot guarantee that a local grid minimum is found. If it were assumed that the simplifications with saved data are required, the allocated space needed for a finer grid search would exceed the radar systems space capacity. A square or finer grid search is therefore not tested, and instead a final NN search is used as an extension of the GN search, so that a local minimum can be guaranteed.

Another aspect needs to be considered is the comparison between each methods STD against true altitude and performance compared to TGS-s. In some cases the optimization algorithm shows less STD then the TGS-s. This will occur

when TGS-s has found the wrong estimate and the optimization algorithm has found the wrong global grid minimum in the LSE-loss matrix. Unfortunately the optimization algorithms estimate is closer to the true altitude, and this is why it gets a lower STD. Therefore this can be misleading when comparing the optimization search methods to the TGS-s. For this matter a better benchmark is to compare the performance column. The STD is however important when TGS-s should be evaluated. The fact that even the TGS-s has less STD than TGS-ns shows two things. Firstly that the measurements are not particularly accurate, but also that the simplified model very well can be used. Meanwhile, the accuracy is rather unimportant for such long range measurements.

In order to reduce the computational burden, a lot of estimates and simplifications are used. Firstly the TGS-s is used as an estimation method, which then is simplified with the pre-saved data, and finally the optimization algorithms are applied. Simultaneous, H_T is estimated from δ_R , after this is used as an estimation parameter, and at last an interpolation between H_T and δ_R is implemented. How much of these estimate and simplifications that are required depend on the computational time for when the algorithm is implemented in a true physical radar system. The computational time depends both on the radars computational power, but also on how the algorithms perform in another programming language. If the result for the mean time is close to the truth, there is a need to save data. It is also easy to conclude that the SD can be rejected since the computational time required is not longer than GN, and still gives worse estimates. Decisions to which of TGS-s, NN, GN or GN with NN that are most appropriate need to be taken after an implementation in a true radar system. For the simulation results the GN with NN though seems to be the one to prefer, since it finds many of the global grid minima and still keeps down the computational burden. Because of the 32 median measurements some errors can be allowed and therefore mean time and flops are important to consider in an evaluation. The space is far away from the actual limit in a radar system and should have a lower impact than all other parameters. If the results for STD with median values between 1.3 to 0.19 km at a target range of 450 km is compared with methods where resolution in angles is analysed this would mean a deviation from 0.16° to 0.02° , which means that all methods have shown good results, despite every estimates and simplifications that are made.

5 CONCLUSION

5.1 Results from Present Work

Conclusions that can be made is that a TGS-ns and SD search can be rejected immediately. Which of the other methods that are most suitable needs to be decided after an implementation is done in a true radar system, but as it seems GN with NN is probably the one to prefer. Trade-offs which should be taken into consideration is primarily between mean time, flops and performance against TGS-s. Because of the 32 median measurements it can be allowed that the algorithms not have found some of the global minima, and the consumed time should have a great impact when a decision should be taken. Having this said one of GN or GN with NN is to prefer. That GN has less STD against true altitude then GN with NN is just a coincidence and is not a good measure of which optimization method to select. This should especially be used when evaluating TGS-s. The allocated space is far from the radars limit and should neither have a great impact in the decision. If an interpolation between H_T and δ_R is to prefer is hard to say, since both reduced time and decreased performance is not changed very much. Despite all estimates and simplifications implemented to reduce the computational time, all methods performance can be regarded as satisfying.

5.2 Future Work

As mentioned, it is difficult to draw any final conclusion about which method that is best. An obvious future work is therefore to make a final implementation in a real radar system. Conclusions can then be taken when methods show their actual performance when implemented in a different programming language.

REFERENCES

- [1] Betts, J. 2001. Practical Methods for Optimal Control Using Nonlinear Programming. Seattle, Washington. [ISBN 0-89871-488-5].
- [2] Blake, L. 1980. Radar Range-Performance Analysis. Norwood, Massachusetts. [ISBN 0-89006-224-2].
- [3] Gratton, S. et al. 2004. Approximate Gauss-Newton methods for nonlinear Least-Squares problems. Numerical analysis report 9. Available: <http://www.henley.ac.uk/web/FILES/maths/09-04.pdf>. Last accessed 15th Mars 2013.
- [4] Hallberg, B. 2001. Radarhöjdmätning med hjälp av modellbaserad signalbehandling. Chalmers Tekniska Högskola. Gothenburg, Sweden.
- [5] Heath, M 2002. Scientific Computing, An Introductory Survey. 2nd Edition. New York, USA [ISBN 0-07-239910-4].
- [6] Kay, S. 1993. Fundamentals of statistical signal processing: Estimation theory, vol. 1. Upper Saddle River, New Jersey. [ISBN 0-13-345711-7].
- [7] McKelvey, T. 2013. On optimization of separable least-squares problems. Gothenburg, Sweden (Supervisor at Chalmers).
- [8] Nathanson, E. 1969. Radar Design Principles, USA. [ISBN 79-80973].
- [9] Råde, L. Westergren, B 2008. Mathematics Handbook Lund, Sweden. [ISBN 91-44-25052-5].
- [10] Skolnik, M. 1990. Radar Handbook. 2nd Edition. USA [ISBN 0-07-057913-x].
- [11] Stimson, G.W. 1988. Introduction to airborne radar. 2nd Edition. New Jersey. [ISBN 1-891121-01-4].

Software

MATLAB and Statistics Toolbox Release 2012b, The MathWorks, Inc., Natick, Massachusetts, United States.